Technical Report

TR-11-08

Literature review on the properties of cuprous oxide Cu_2O and the process of copper oxidation

P A Korzhavyi, B Johansson
Department of Materials Science and Engineering
Royal Institute of Technology

October 2011

Svensk Kärnbränslehantering AB
Swedish Nuclear Fuel
and Waste Management Co

Box 250, SE-101 24 Stockholm
Phone +46 8 459 84 00

ISSN 1404-0344
SKB TR-11-08

Literature review on the properties of cuprous oxide Cu_2O and the process of copper oxidation

P A Korzhavyi, B Johansson
Department of Materials Science and Engineering
Royal Institute of Technology

October 2011

Abstract

The purpose of the present review is to provide a reference guide to the most recent data on the properties of copper(I) oxide as well as on the atomic processes involved in the initial stages of oxidation of copper. The data on the structure of surfaces, as obtained from atomic-resolution microscopy studies (for example, STM) or from first-principles calculations, are reviewed. Information of this kind may be useful for understanding the atomic mechanisms of corrosion and stress-corrosion cracking of copper.

Introduction

The name “cuprite” of cuprous oxide Cu_2O comes from the Latin “cuprum”, meaning copper. Old miners used to call it “ruby copper”. Cuprite mineral has been a major ore of copper and is still mined in many places around the world. Of all the copper ores, except for native copper, cuprite gives the greatest yield of copper per molecule since there is only one oxygen atom to every two copper atoms. As a mineral specimen, cuprite shows fine examples of well-developed cubic crystal forms. Crystal habits include the cube, octahedron, dodecahedron, and combinations of these forms. Cuprite’s color is red to a deep red that can appear almost black. Dark crystals show internal reflections of the true deep red inside the almost black crystal. Other varieties, such as chalcotrichite, form long needle-like crystals that have a beautiful red color and a special sparkle that make them popular display cabinet specimens.

Cuprite (or cuprous oxide) is the oldest material of semiconductor electronics (Brattain 1951). It has been the subject of numerous theoretical and experimental studies, but still its electronic and atomic structures continue to puzzle the researchers. New applications of Cu_2O in nanoelectronics, spintronics, and photovoltaics are emerging. However, our present interest in this material is motivated by the fact that Cu_2O is a commonly occurring corrosion product of copper. Understanding cuprite at the electronic and atomic structure levels may be useful for predicting and controlling the corrosion behavior of copper.

Contents

1 Atomic and electronic structure 9
1.1 Crystallography and lattice stability 9
1.2 Electronic structure 10
1.2.1 Electronic spectra and optical properties 10
1.2.2 Charge density and bonding in cuprite 12
1.2.3 Cohesive properties 13
1.2.4 Electrical properties and photoconductivity 16
1.3 Details of calculations 17

2 Point defects and electronic properties 19
2.1 Diffusion and electrical conductivity data 19
2.2 Nonstoichiometry in Tretyakov's model 20
2.3 Thermal disorder in Bloem's model 21
2.4 Defect structure model by Peterson and Wiley 22
2.5 Defect structure model by Xue and Dieckmann 22
2.6 Mobile charged defects in the model by Park and Natesan 23
2.7 Defect structure model by Porat and Riess 23
2.8 Other defect models of cuprite 24
2.9 Present *ab initio* calculations 24
2.10 Nature of *p*-type conductivity of Cu_2O 26
2.11 Hydrogen in cuprite 27

3 Initial stages of copper oxidation 29
3.1.1 Cu(100) surface 29
3.1.2 Cu(115) and Cu(119) surfaces 31
3.1.3 Cu(110) surface 31
3.1.4 Cu(111) surface 32
3.2 Oxidation in aqueous solutions 32
3.2.1 Cu(100) surface 32
3.2.2 Cu(110) surface 33
3.2.3 Cu(111) surface 33
3.3 Surfaces of Cu_2O 34

Conclusions 35

Acknowledgments 35

References 37

1 Atomic and electronic structure

1.1 Crystallography and lattice stability

Cuprite crystallizes in a simple cubic structure which can be viewed as two sublattices, a face-centered cubic (fcc) sublattice of copper cations and a body-centered cubic (bcc) sublattice of oxygen anions. The oxygen atoms occupy tetrahedral interstitial positions relative to the copper sublattice, see Figure 1-1, so that oxygen is tetrahedrally coordinated by copper, whereas copper is linearly coordinated by two neighboring oxygens. These low coordination numbers are very unusual for metal oxides (only by two other substances, Ag_2O and Pb_2O, have this crystal structure). Also, a short copper-oxygen bond length in Cu_2O is unusual, see Table 1-1, it is not compatible with the sum of any pair of the ionic radii for Cu^+ and O^{2-} given in the literature[1].

Table 1-1. Crystallographic parameters of copper oxides according to Wells (1984) and Åsbrink and Norrby (1970).

	Cu_2O	CuO
	Cubic	Monoclinic
Lattice parameters	a = 4.27 Å	a = 4.6837 Å
		b = 3.4226 Å
		c = 5.1288 Å
		β = 99.54°
Shortest distances		
$d_{Cu\text{-}O}$	1.84 Å	1.95 Å
$d_{O\text{-}O}$	3.68 Å	2.62 Å
$d_{Cu\text{-}Cu}$	3.02 Å	2.90 Å

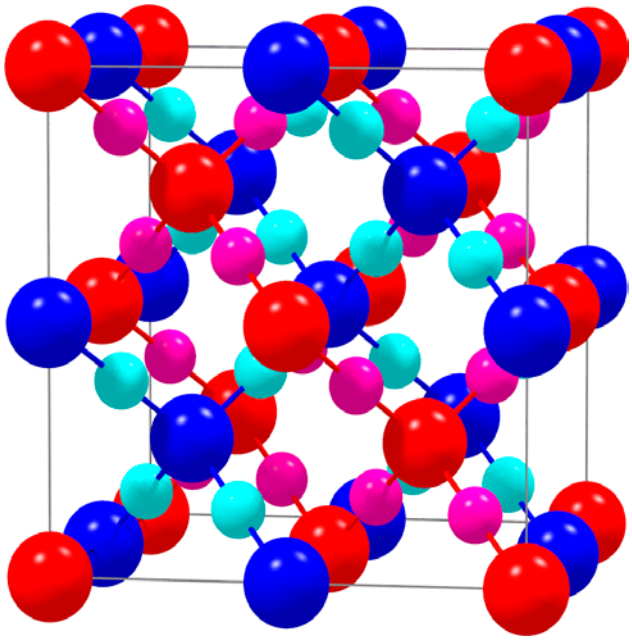

Figure 1-1. *Ball-and-stick representation of cuprite (Cu_2O) crystal structure, where linearly coordinated copper cations are shown as small balls and tetrahedrally coordinated oxygen anions – as large balls. The split-up of the structure into two disconnected anti-SiO_2 (cristobalite) networks is indicated by color: one network is colored pink and red, whereas the other – magenta and blue.*

[1] Values of ionic radii are given by several authors: Cu^+: r = 0.96 Å (Pauling), O^{2-}: r = 1.32 Å (Goldschmidt), r = 1.40 Å (Pauling). The sum of the Cu^+ and O^{2-} ionic radii is 2.28 (2.36) Å; the Cu-O distance in Cu_2O is 1.84 Å. Although this interatomic distance can be reproduced using coordination-dependent ionic radii (Shannon 1976), one has to accept an extremely small radius value, 0.46 Å, for the doubly coordinated Cu^+ ion.

Another interesting feature of the cuprite structure is its dichotomy. As illustrated in Figure 1-1, the structure may be viewed as consisting of two identical interpenetrating networks, each having the same anti-SiO_2 (cristobalite) structure. If one uses a ball-and-stick model to indicate the ionic-covalent nearest-neighbor bonds between the O^{2-} and Cu^{+} ions, it turns out that there are no primary (chemical) bonds connecting the two cristobalite networks together. The networks are forced to their respective places by secondary (physical, van der Waals) forces, arising due to dispersive electrostatic interactions. On the other hand, these electrostatic interactions are relatively weak, and mostly repulsive, so that the two networks are *loosely bound*. This fact may be linked to several anomalies of the physical properties of Cu_2O (and of Ag_2O having the same structure):

- From the set of experimentally measured (Hallberg and Hanson 1970) elastic constants of Cu_2O at −269°C ($C_{11} = 121 \pm 5$, $C_{12} = 105 \pm 4$, and $C_{44} = 10.9 \pm 0.3$ GPa) one concludes that the resistance of cuprite structure to shear [characterized by constants C_{44} and $C' = (C_{11} - C_{12})/2 \cong 8$ GPa] is very low compared to the bulk modulus of cuprite, $B = (C_{11} + 2C_{12})/3 \cong 110$ GPa. This result implies that it is easier to shift one network with respect to the other than to vary the Cu-O bond length.
- Both shear constants C_{44} and C' of Cu_2O *increase* with increasing temperature (Hallberg and Hanson 1970, Manghnani et al. 1974). Thus, room-temperature (20°C) values of the elastic constants of Cu_2O are $C_{11} = 116.5$, $C_{12} = 100.3$, and $C_{44} = 12.14$ GPa (from which one deduces that $C' = 8.1$ GPa) (Hallberg and Hanson 1970).
- Cu_2O (below 200 K) and Ag_2O (up to its decomposition temperature of about 500 K) exhibit negative thermal expansion (NTE) (Schäfer and Kirfel 2002, Tiano et al. 2003, Dapiaggi et al. 2003, Fornasini et al. 2006, Mittal et al. 2007).

In order to explain the stability of cuprite structure against shear (i.e. why the shear constants are positive), one has to perform a detailed consideration of the electronic structure of Cu_2O, including so-called "closed-shell" or "dispersive" interactions between the two cristobalite networks. In many compounds, the Cu(I) and Ag(I) cations also adopt close-packed and related configurations with short metal-metal distances that are strongly suggestive of the occurrence of the metal-metal bonding, despite their formal nd^{10} electron configuration. Such observations have been explained by invoking the participation in bonding of electron orbitals of higher principal quantum number – that is, $(n+1)s$ and $(n+1)p$ – accompanied by the creation of d-orbital holes on the metal atoms (Orgel 1958). These assumptions were later corroborated by accurate electronic structure calculations (Marksteiner et al. 1986), and d-orbital holes were even "seen" in experiment (Zuo et al. 1999, Humphreys 1999). Let us now review the results of recent studies of the electronic structure of Cu_2O, with the emphasis on the nature of chemical bonding in this compound.

1.2 Electronic structure

The electron energy bands of Cu_2O have been extensively studied (Zuo et al. 1999, Kleinman and Mednick 1980, Robertson 1983, Marksteiner et al. 1986, Ghijsen et al. 1988), mainly because of its unusual exciton spectrum [cuprite exhibits a long series of exciton transitions, beginning with a forbidden line (Elliott 1957, 1961)]. There are some other aspects of electronic structure of cuprite that are interesting from a theoretical point of view. For instance, non-cubic symmetry of the local coordination of Cu cations in this compound causes a non-vanishing electric field gradient on the Cu nuclei, quite uncommon a situation for cubic structures (Marksteiner et al. 1986). Since the crystal structure of cuprite combines high overall symmetry with low symmetry of local coordination, it has also been used as a benchmark system to test computer codes for electronic structure calculations (Madsen et al. 2001). In this section, we will mainly concentrate on the results of those studies, which are related to nature of chemical bonding in cuprite. At the end of the section, the results of the present study will also be discussed.

1.2.1 Electronic spectra and optical properties

Extensive experimental studies of the electronic spectra of Cu_2O have been performed, including photoelectron spectroscopy (PES) (Ghijsen et al. 1988, Hu et al. 2008b, Shen et al. 1990, Önsten et al. 2007), Auger electron spectroscopy (Ghijsen et al. 1988, Barman and Sarma 1992), and optical adsorption and photoluminescence spectroscopy (Baumeister 1961, Taylor and Weichman

1969, Uihlein et al. 1981, Jolk and Klingshirn 1998, Boucher 2005b). The effects of structural disorder (associated with the oxygen content in cuprite) on the optical (Boucher 2005b) and electrical (Boucher 2005a) properties of Cu_2O have been investigated. Infrared and Raman spectra of Cu_2O have been measured (O'Keeffe 1963, Dawson et al. 1973, Yu and Shen 1975, 1978, Ivanda et al. 1997, Burlakov et al. 1999, Serin et al. 2005). Phonon spectra of cuprite have been studied in detail by means of inelastic neutron scattering measurements (Mittal et al. 2007, Beg and Shapiro 1976, Bohnen et al. 2009). It can be noted that the new neutron scattering data obtained by Bohnen et al. (2009) seem to be more accurate and should be used instead of the old data by Beg and Shapiro (1976).

The electron and phonon spectra of Cu_2O have been investigated theoretically, using local and semi-local functionals of DFT (density functional theory) based calculations (Zuo et al. 1999, Kleinman and Mednick 1980, Marksteiner et al. 1986, Ghijsen et al. 1988, Ching et al. 1989, Madsen et al. 2001, Martínez-Ruiz et al. 2003, Laskowski et al. 2003, Mittal et al. 2007, Soon et al. 2006, 2007a, b, 2009, Bohnen et al. 2009, Islam et al. 2009a, Önsten et al. 2007, Korzhavyi and Johansson 2010, Korzhavyi et al. 2011), as well as through calculations employing more advanced schemes such as Hartree-Fock (Wang and Schwarz 2000, Ruiz et al. 1997), DFT+*U* (Laskowski et al. 2003, Sieberer et al. 2007, Nolan and Elliott 2006, Raebiger et al. 2007, Önsten et al. 2007), pseudo-SIC (self-interaction correction) (Filippetti and Fiorentini 2005a), the so-called *GW* approximation (Bruneval et al. 2006, Dash et al. 2007), and hybrid exchange formalism (Hu et al. 2008b, Scanlon and Watson 2011).

A very important issue to be addressed first is how well these self-consistent electronic structure calculations, based on density functional theory (DFT), can reproduce the experimentally observed electronic structure of this compound. A detailed comparison of the experimental X-ray and ultraviolet photoemission spectra (XPS and UPS), Auger electron spectra, and Bremsstrahlung isochromat spectra (BIS) of Cu_2O and CuO with the electron spectra calculated using the localized augmented-spherical-wave (ASW) method can be found in Ref. Ghijsen et al. (1988). Good agreement between the measured spectra and calculated (broadened) densities of occupied and unoccupied states is found in both cases (Cu_2O and CuO), except for constant energy shifts needed to match the experimental and calculated band edges. This kind of agreement is reasonable to expect for Cu_2O, which has an essentially full 3*d* shell. CuO has an open *d* shell ($3d^9$) and, according to experiment, it is an antiferromagnetic semiconductor with a gap of about 1.4 eV, whereas existing DFT calculations predict it to be a non-magnetic metal[2].

Another important parameter of the energy spectrum of Cu_2O is the energy gap. Cu_2O represents a much studied textbook example of a semiconductor with a gap of 2.17 eV. The energy gap value has immediate implications for the energetics of point defects in semiconductors (Kröger 1964). The experimental gap value is compared with *ab initio* calculated values in Table 1-2. As follows from the table, self-consistent electronic structure calculations performed using LDA or GGA exchange-correlation potential give only about one-third of the experimental energy gap in Cu_2O. Taking into account the gradient corrections to the exchange-correlation potential (i.e. using the GGA instead of the LDA potential) does not improve on the energy gap. On the other hand, Hartree-Fock calculations (Ruiz et al. 1997) give by far too wide a band gap for Cu_2O. Self-interaction corrected (SIC) calculations, which are still using a first-principles approach, give a band gap value of 1.8 eV, which is still far from the experimental value. In the GGA+*U* calculations by Raebiger et al. (2007) employed values U=7 eV and J=1 eV as fitting parameters to reproduce the experimental band gap. A similar fitting procedure was employed in the hybrid functional calculations of Ref. Hu et al. (2008b).

[2] The reasons for these discrepancies are the same as those responsible for the failure of band theory in NiO and CoO. Namely, the existing approximations for the exchange-correlation potential in density functional theory, the local density approximation (LDA), and generalized gradient approximation (GGA), are still too crude to reproduce all the details of the electronic structure of these materials. A similar problem has been found in the description of high-temperature superconductor material $YBa_2Cu_2O_{7-x}$, where Cu atoms in the CuO_2 planes are known to form antiferromagnetic order, whereas electronic structure calculations, which use either LDA or GGA, give zero magnetic moments on these Cu sites. It is noteworthy that the ground-state properties of these materials, which derive from total energy, are usually reproduced very well, especially within the GGA.

Table 1-2. *Ab initio* calculated and experimental values of the energy gap in semiconductor Cu_2O. Calculated values are obtained at the experimental lattice parameter, a_0 = 4.27 Å.

Method	Exchange-correlation	Reference	E_i, eV
Experiment		Kittel (1986)	2.17
Gaussian orbitals	LDA	Kleinman and Mednick (1980)	1.07
FP-LAPW [a]	LDA	Marksteiner et al. (1986)	0.60
FP-LAPW	GGA	Martínez-Ruiz et al. (2003)	0.60
Dmol^3 [b]	GGA	Soon et al. (2006)	0.64
Dmol^3	GGA	Soon et al. (2009)	0.46
FP-LMTO [c]	LDA	This work	0.54
FP-LMTO	GGA	This work	0.55
KKR-ASA+M [d]	LDA	This work	0.56
QE [e]	GGA	This work	0.53
VASP-PAW [f]	LDA	Filippetti and Fiorentini (2005a)	0.55
VASP-PAW	GGA	Raebiger et al. (2007)	0.43
VASP-PAW	GGA	Islam et al. (2009a)	0.70
VASP-PAW	LDA+SIC	Filippetti and Fiorentini (2005a)	1.80
VASP-PAW	GGA+*U*	Raebiger et al. (2007)	2.10
AbInit	sc*GW* [g]	Bruneval et al. (2006)	1.97
CRYSTAL	HF+LYP [h]	Ruiz et al. (1997)	9.70
CRYSTAL	Hybrid	Hu et al. (2008b)	2.10
VASP-PAW	Hybrid	Scanlon and Watson (2011)	2.12

[a] Full-potential, linearized augmented plane wave method.

[b] Density-functional program for molecules and solids.

[c] Full-potential, linearized muffin-tin orbital method.

[d] Korringa-Kohn-Rostoker method, multipole-corrected atomic sphere approximation.

[e] Quantum Espresso, a plane-wave pseudopotential code.

[f] Vienna *ab initio* simulation package, the projector augmented wave method.

[g] Self-consistent *GW* approach.

[h] Hartree-Fock method plus *a posteriori* correlation energy correction using the Lee-Yang-Parr functional.

Bruneval et al. (2006) and Dash et al. (2007) have extended a recently proposed self-consistent quasiparticle approach, based on the *GW* approximation, to the calculation of optical spectra, including excitonic effects, in Cu_2O. The band structure compares favorably with the angle-resolved photoemission measurements reported in the same papers. The excitonic effects (derived from the realistic band structure and screening) provide a reliable optical absorption spectrum, which allows for a revised interpretation of its main structures. A general conclusion may be drawn from the reviewed studies (Filippetti and Fiorentini 2005a, b, Bruneval et al. 2006, Dash et al. 2007, Nolan and Elliott 2006, Raebiger et al. 2007, Önsten et al. 2007) that one gets a fairly good description of the electronic and magnetic structure, as well as of the optical properties and defect chemistry, of copper oxides if one goes beyond the standard DFT scheme.

1.2.2 Charge density and bonding in cuprite

Let us now discuss the features of chemical bonding in Cu_2O and also interconnection between the electronic and crystal structure of this compound. Many theoretical calculations of the charge density in cuprite have been published (Wang and Schwarz 2000, Marksteiner et al. 1986, Ruiz et al. 1997, Madsen et al. 2001, Laskowski et al. 2003, Filippetti and Fiorentini 2005a). It is usually found that the charge densities at copper and oxygen are not spherically symmetric, but the charge density plots are given different interpretations in different studies. If one interprets the degree of non-sphericity as a measure of Cu-O bond covalency, then one finds that DFT (density functional theory) calculations (Marksteiner et al. 1986, Madsen et al. 2001, Laskowski et al. 2003) typically predict a higher degree of covalency (as opposed to ionicity) in Cu_2O, as compared to the Hartree-Fock (Wang and Schwarz 2000, Ruiz et al. 1997) or DFT+*U* (Laskowski et al. 2003, Filippetti and Fiorentini 2005a) calculations.

Marksteiner et al. (1986) were first to discuss the deviations from standard ionic model for Cu_2O in terms of electron density difference plots, where the superimposed electron density of Cu^+ [$3d^{10}4s^0$] and O^{2-} ions had been subtracted from the self-consistent, crystalline charge density of Cu_2O. The difference was found to be quite small and spherically symmetric around the oxygen atom. Therefore, it is justified to speak about an O^{2-} anion. However, the difference around the Cu atom was found to be non-spherical. The negative calculated difference around Cu suggests an incompletely filled *d*-shell, the missing charge being transferred into the interstitial region. Certain degree of hybridization between the 4*sp* and 3*d* states on Cu ions has been suggested to be responsible for this effect. As a result, some of the *d*-states (having d_{z^2} orbital character) on Cu ions remain unoccupied. These empty states have been observed experimentally (Zuo et al. 1999) as hole "clouds", which are centred on Cu ions and elongated in the [111] O-Cu-O direction. However, the measured hole density seems to be much greater than the calculated (Marksteiner et al. 1986) density of holes. This discrepancy may be ascribed to non-stoichiometry or thermal point defect disorder in the experimental Cu_2O sample. These effects are known make this compound an intrinsic *p*-type semiconductor, see next chapter.

Accurate experimental measurements of the electron density distribution in cuprite Cu_2O have been performed using a low-energy (Kirfel and Eichhorn 1990) and a high-energy (Lippmann and Schneider 2000a, b) synchrotron radiation sources. They provide a picture of bonding in Cu_2O which is similar to the theoretical picture except, perhaps, for somewhat stronger ionicity of bonding (Lippmann and Schneider 2000b). However, these studies do not confirm the density maximum at the tetrahedral interstitial position reported by Zuo et al. (1999). The maximum is suspected (Wang and Schwarz 2000) to be due, most probably, to the presence of defects (interstitial impurities and/or copper vacancies) in the experimental sample. Contrary to the conclusions of Ref. Zuo et al. (1999), the nature of closed-shell (Cu^+[$3d^{10}4s^0$]) interactions between the cristobalite networks does not require any maximum of electron density in the center of unoccupied Cu_4 tetrahedron (Lippmann and Schneider 2000b, Wang and Schwarz 2000, Buljan et al. 2001, Laskowski et al. 2003).

Filippetti and Fiorentini (2005a) have investigated the nature of bonding in noble-metal oxides using a combination of first-principles density functional based methodologies including self-interaction correction, polarization theory, and the electron localization function. The authors give a detailed and consistent picture of bonding in Cu_2O (and related compounds) at some variance with that hitherto assumed. First, they see no trace of interstitial covalency, thereby negating the covalent bonding hypothesis. Second, the authors show that the cation on-site *s-d* hybridization causes only a marginal deviation from the exact sphericity of the electron charge and contributes negligibly to the stabilization of the cubic phase. Third, they show that the cubic phase is stable because of incomplete ionic charge transfer, leaving on the cation an excess of delocalized charge which establishes weakly metallic cation-cation bonding.

In their other work Filippetti and Fiorentini (2005b) investigate the interplay of bonding and magnetism in CuO by a first-principles self-interaction free density-functional approach. Their analysis reveals that, at variance with typical low-dimensional cuprates, a fully three-dimensional view of the exchange interactions is needed to accurately describe the magnetic ground state and low-energy excitations in CuO. The apparent one-dimensional behavior of antiferromagnetic order is found to be due to the presence of a single spin-polarized hole of d_{z^2} character. This induces a strongly anisotropic magnetic ordering built up by ferromagnetic (*x*;*y*) layers, and antiferromagnetic chains along *z*, with exchange interactions of similar magnitude.

1.2.3 Cohesive properties

Although quite many electronic structure calculations have been done for Cu_2O, the information on the calculated cohesive properties of this compound is scarce. In this connection, in the present work we have performed calculations of the equilibrium lattice parameter, bulk modulus, and pressure derivative of the bulk modulus of Cu_2O, using several electronic structure methods, including a most accurate all-electron full-potential linearized muffin-tin orbital (FP-LMTO) method, which we use as a benchmark method. We also employ a plane-wave based code Quantum Espresso (QE) (Baroni et al. 2001), together with ultrasoft pseudopotentials (Vanderbilt 1990), in order to calculate the electronic and phonon spectra of Cu_2O, as well as evaluate its thermodynamic properties at finite temperatures within the quasiharmonic approximation. The details of our calculations will be described in Section 1.3. The calculated results are presented and compared with the literature data in Table 1-3 and Table 1-4.

Table 1-3. *Ab initio* calculated cohesive properties of Cu_2O: Lattice parameter a_0 , bulk modulus B, and pressure derivative of the bulk modulus, $B' = dB/dP$. In all these calculations the atomic nuclei (ions) were treated as static. Abbreviations are the same as in Table 1-2.

Method	Technique	a_0, Å	B, GPa	B'	Reference
Experiment	Ultrasonics	4.27	110–112	4.5	Hallberg and Hanson (1970), Manghnani et al. (1974)
Experiment	High-pressure		131	5.7	Werner and Hochheimer (1982), Smyth et al. (2000)
CRYSTAL	HF+LYP	4.28	93		Ruiz et al. (1997)
FP-LAPW	GGA	4.31	112		Laskowski et al. (2003)
FP-LAPW	GGA+U	4.20	139		Laskowski et al. (2003)
FP-LMTO	LDA	4.18	137	4.6	This work
FP-LMTO	GGA	4.33	104	4.6	This work
KKR-ASA+M	GGA	4.29	105	4.8	This work
QE	GGA	4.30	120	4.8	This work

Table 1-4. Experimental and calculated lattice parameters a of Cu_2O at 0 K (including the zero-point energy of ionic motion) and at room temperature (RT), T = 298.15 K. Standard enthalpy of formation ΔH calculated relative to Cu and O_2 in their standard states at RT. All the calculated results are obtained within the GGA (Perdew et al. 1996). Abbreviations are the same as in Table 1-2.

Method	a(0 K), Å	a(273 K), Å	ΔH, kJ·mol^{-1}	Reference
Experiment	4.272	4.270	171	Tiano et al. (2003), Chase (1998).
Experiment	4.276	4.275		Schäfer and Kirfel (2002).
Dmol^3 (static ion)	4.32		120	Soon et al. (2006, 2007a, 2009).
QE	4.303	4.304	113	This work.

The FP-LMTO results, which have been obtained using a minimum number of approximations, show a well-known tendency of the LDA to underestimate the lattice parameter and to overestimate the bulk modulus. The gradient corrections, included within the GGA, improve on the lattice parameter, but seem to over-correct the bulk modulus, so that its value calculated within the GGA is lower than the experimental values. The overall agreement between theory and experiment is quite encouraging for the cohesive properties, despite the fact that the dielectric energy gap of Cu_2O is strongly underestimated by all the methods used. Interestingly, all the methods give value in the range 4.6–4.8 for the pressure derivative of the bulk modulus of Cu_2O, which is close to the $B' = 4.5$ obtained in ultrasonic measurements (Manghnani et al. 1974) of the elastic constants in cuprite, whereas the other experimental value is somewhat higher. Also, it seems that the experimental value of the bulk modulus obtained by Manghnani et al. (1974) is in better agreement with the calculated values, whereas the bulk modulus obtained in the high-pressure studies of Werner and Hochheimer (1982) and Smyth et al. (2000) is considerably higher. This apparent disagreement between the two sets of experimental results can be attributed to the effect of strengthening of the crystal by lattice defects.

Moss et al. (1988) find that mineralogical form of cuprite is more rigid than annealed or synthetic cuprite crystals, due to the presence of copper-deficient (100) fault planes in the mineralogical form. This result can be understood if one takes into account that the two cristobalite networks of the cuprite structure are disconnected only in the absence of defects. Presence of defects creates primary chemical bonds between the two networks, which are otherwise bound by secondary (dispersive) interactions, which are by an order of magnitude weaker than primary chemical (covalent or ionic) interactions. Of course, the defects increase total energy of the structure, but, at the same time, they make the lattice more rigid.

The phonon spectrum of Cu_2O, calculated at the experimental room-temperature lattice parameter, is presented in Figure 1-2 in comparison with experimental data. The vibrational spectrum of Cu_2O consists of two groups of phonon states (low- and high-frequency states) separated by a gap. The high-frequency states are due to optical modes of oxygen, whereas the low-frequency states are due to acoustic modes and optical modes associated with Cu.

Similar phonon spectra were calculated for a set of volumes near the equilibrium volume (quasi-harmonic approximation); their integration yielded thermal properties of cuprite such as the heat capacity, free energy, and thermal expansion. The so calculated thermal expansion coefficient and heat capacity of cuprite are shown in Figure 1-3, in comparison with experimental data. The present calculations, based on linear response theory, are able to reproduce in every detail the unusually complex shape of the C_P curve of cuprite, as well as to explain it by the split-up of the phonon spectrum onto the low- and high-frequency states.

Also, our calculations reproduce (on a semi-quantitative level) a thermal expansion anomaly of cuprite: Cu_2O is known to have a low value of thermal expansion coefficient around room temperature, and to exhibit negative thermal expansion coefficients at low temperatures. Negative thermal expansion is characteristic of materials with saturated type of interatomic bonding (e.g. semiconductors or organic materials) having open structures (for example, containing long chains of atoms). The frequencies of transverse vibrations of such chains are typically rather low when the chain is relaxed, but the frequencies increase the chain is stretched, similar to the tune of a guitar string. In metals, or in other densely-packed solids, the frequencies corresponding to three-dimensional, "bulky" atomic configurations typically *decrease upon expansion*.

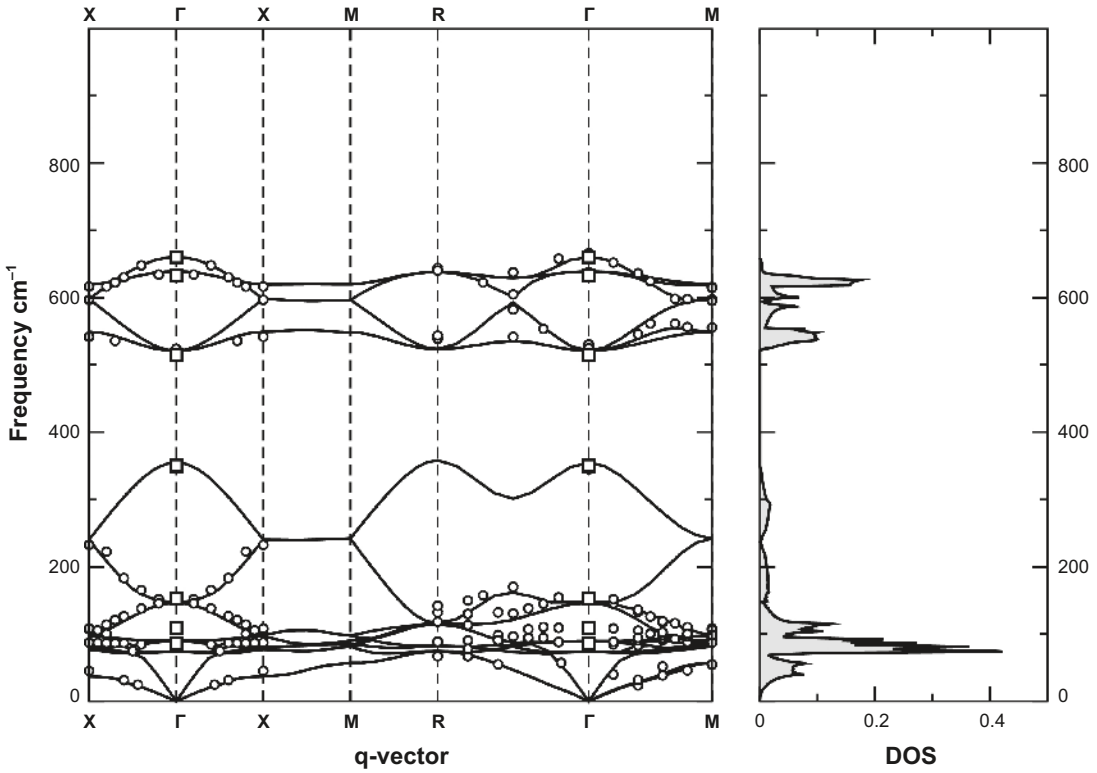

Figure 1-2. *Phonon spectrum and density of states (DOS) in cuprous oxide, Cu_2O, calculated at the experimental lattice parameter a_0 = 4.27Å. Experimental data on inelastic neutron scattering (Bohnen et al. 2009) and Raman scattering (Yu and Shen 1975) are shown, respectively, as open circles and open squares.*

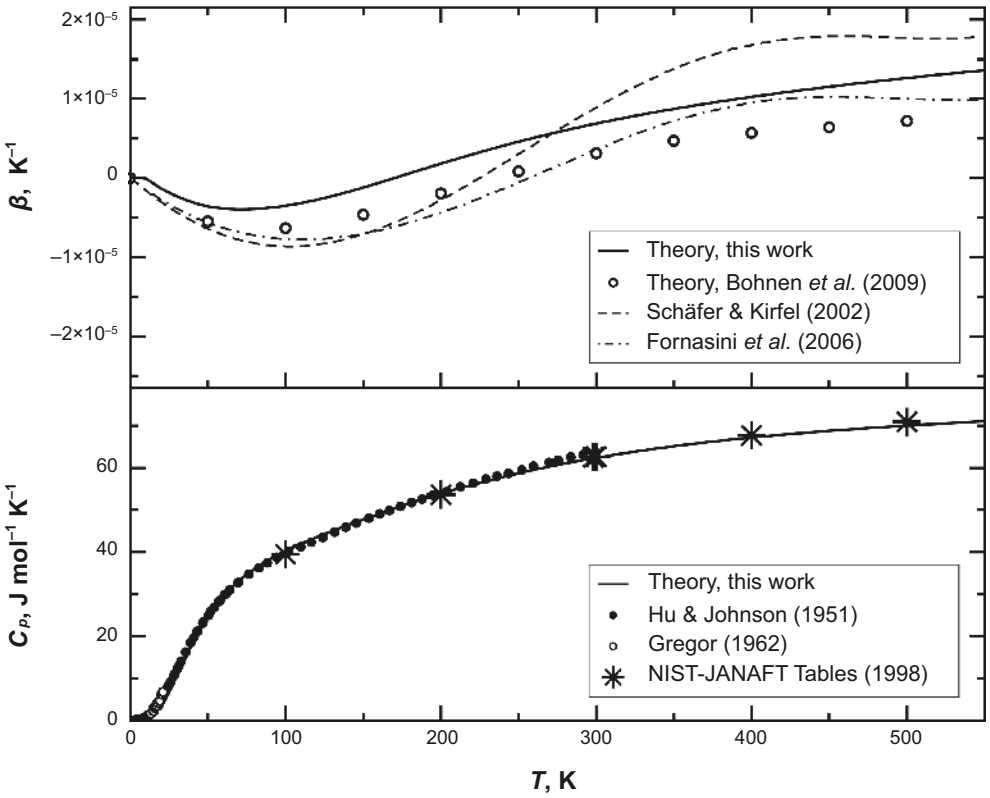

Figure 1-3. *Thermal properties of Cu_2O: thermal coefficient of volume expansion β (upper panel) and heat capacity C_P (lower panel), calculated within the quasiharmonic approximation for the phonon part of free energy. Experimental data on are taken from Refs. Schäfer and Kirfel (2002), Fornasini et al. (2006) (thermal expansion) and Refs. Hu and Johnston (1951), Gregor (1962), Chase (1998) (heat capacity).*

However, in Cu_2O there are low-lying transverse acoustic modes (such as, for example, zone-boundary acoustic modes at point X that correspond to a twist of corner-sharing Cu_4O tetrahedra with respect to each other (Mittal et al. 2007)) whose frequencies *decrease upon compression*. Therefore, at low temperatures, the structure will gain some additional vibrational entropy by shrinking the volume so that the cristobalite networks consisting of corner-sharing Cu_4O tetrahedra become misoriented (and the O-Cu-O chains become loose) so the corresponding frequencies decrease. When the temperature exceeds a certain threshold, higher-lying modes become excited whose frequencies decrease upon expansion, and the thermal expansion behavior returns to normal (Bohnen et al. 2009, Korzhavyi and Johansson 2010, Korzhavyi et al. 2011).

1.2.4 Electrical properties and photoconductivity

Original experimental data and recent research papers on the electrical and photoelectrical properties of Cu_2O can be found in Refs. Weichman (1960), Schick and Trivich (1971), Rakhshani (1986), Rai (1988), Musa et al. (1998). The Reader is referred to Ref. Ito et al. (1998) for a recent review.

In addition to the original interest to Cu_2O as a low-cost material for solar cells (Olsen et al. 1982), a new potential application area of cuprite (as a photocatalist for hydrogen production from water) is being actively explored. Cu_2O was recently found to produce overall water splitting, i.e. into H_2 and O_2, under the action of visible light (Hara et al. 1998, Ikeda et al. 1998). Later, more accurate analyses showed that, under open-cirquit conditions, Cu_2O is unstable with respect to further oxidation to form CuO (de Jongh et al. 1999, Walker and Yates 2000, Brown and Choi 2006, Kakuta and Abe 2009). At photocatodic conditions, however, cuprite shows a long-term stability and a surprisingly high quantum efficiency for the photocathodic reduction of oxygen (de Jongh et al. 1999). Therefore Cu_2O could be a promising material, not for direct photoelectrochemical water splitting, but in conjunction with a suitable redox system as a *p*-type photoelectrode in an electrochemical photovoltaic cell (de Jongh et al. 1999, Siripala et al. 2003, Bessekhouad et al. 2005, Somasundaram et al. 2007, Hu et al. 2008a).

1.3 Details of calculations

Here we list the main parameters of our electronic structure calculations using which the results presented in Section 1.2 have been obtained. The calculations were based on density functional theory (Hohenberg and Kohn 1964, Kohn and Sham 1965) and employed several band structure methods.

FP-LMTO. The full-potential linearized muffin-tin orbital method (Andersen 1975) calculations were done using the LmtART software package developed by S. Y. Savrasov (Savrasov and Savrasov 1996, Savrasov 1996). In the LDA calculations, the Vosko-Wilk-Nusair parametrization (Vosko et al. 1980) of the exchange-correlation potential was used, the gradient correction terms according to Perdew, Burke, and Ernzerhof (Perdew et al. 1996) (PBE) were included in the GGA calculations. A two-κ MTO basis set was used for the valence states. The wave functions inside the muffin-tins were expanded in spherical harmonics with a cutoff $l_{max} = 2$ for Cu and $l_{max} = 1$ for O, whereas a plane-wave representation (on a 40×40×40 or 50×50×50 Fourier grids in the LDA or GGA calculations, respectively) was used in the interstitial region. The Brillouin zone (BZ) integrations were carried out by means of the improved tetrahedron method (Blöchl et al. 1994), using 20 **k**-points in the BZ irreducible wedge of the simple cubic structure. Core states were recalculated at each self-consistency loop.

Quantum-Espresso (QE). The electronic and phonon structure of Cu_2O was calculated using the Quantum-Espresso software package (Giannozzi et al. 2009). The calculations were based on density-functional perturbation theory (Baroni et al. 2001) and employed the Vanderbilt ultra-soft pseudopotentials (Vanderbilt 1990) together with the generalized gradient approximation (Perdew et al. 1996). The thermodynamic properties of Cu_2O at $T = 0$ K and at finite temperatures were evaluated from the calculated total energies and phonon spectra of Cu_2O using the quasi-harmonic approximation (Baroni et al. 2010).

KKR-ASA+M. The Korringa-Kohn-Rostoker (KKR) Green's function method (Ruban and Skriver 1999, Abrikosov et al. 1997) has been used for electronic structure calculations of perfect and defected Cu_2O. The calculations employed the PBE exchange-correlation potential (Perdew et al. 1996), as well as the multipole-corrected atomic sphere approximation (Korzhavyi et al. 1999) (ASA+M). Since the ASA may severely affect the accuracy of calculations in cases of loosely packed structures (due to large overlap of the atomic spheres), we have reduced the overlap by adding "empty spheres" – which contain no nuclear charge – in the unoccupied tetrahedral and octahedral sites of the fcc sublattice of Cu (Wyckoff positions 4*c* and 6*d*). The sphere radii for the Cu atoms and for the octahedral positions were chosen to be equal to each other and 1.11 times as large as the sphere radii for O atoms and for the tetrahedral positions. The basis functions have been expanded up to $l_{max} = 3$ (*spd*-basis) inside the atomic and empty spheres, while the multipole moments of the electron density have been calculated up to $l^{M}_{max} = 4$. The Green's function integration over energy was performed in the complex energy plane on a semicircular contour using a Gaussian grid comprised of 25 points. The Brillouin zone integration was done on a grid of k-points uniformly distributed in the irreducible wedge of BZ (165 points). The core states were recalculated at each self-consistency loop.

2 Point defects and electronic properties

The presence of point defects in crystals at equilibrium may be either due to nonstoichiometry (in such a case the defects are called *constitutional* defects) or due to temperature-induced disorder (such defects are called *thermal* defects). Real crystals at finite temperatures possess certain amount of both constitutional and thermal defects. Deviations from the equilibrium defect concentrations may be produced by, for instance, sudden temperature changes, mechanical deformation, irradiation, or chemical doping. All these equilibrium and non-equilibrium point defects have important influence on the physical properties of compounds. Cu_2O was among the first solids for which a dependence of the optical and electric properties on the conditions of preparation (partial oxygen pressure, P_{O_2}, and temperature) was observed. For references see Kröger (1964).

Theoretical modeling of point defects in crystals was pioneered by Wagner and Schottky (1930), who established the connection between imperfections in the crystal lattice and the nonstoichiometry. The Wagner-Schottky (WS) model was, however, too simple to describe the disorder in ionic or covalent crystals. The WS model was further developed by Shockley and Last (1957), and by Kröger (1964), in order to incorporate into the model the effects of electronic structure, i.e. the fact that formation of point defects may be accompanied by the creation/annihilation of electrons and holes. A detailed review of this so-called quasichemical method, as well as of its applications to various systems can be found in the classical book by Kröger (1964).

In this Chapter, the experimentally derived models of point-defect disorder will be discussed and compared with the results of the total energy calculations for nonstoichiometric Cu_2O performed in this work and in other theoretical studies. The following notations for the atomic defect species will be used throughout the text:

V_{Cu} – vacancy on the copper sublattice;

V_O – vacancy on the oxygen sublattice;

Cu_O – antisite Cu atom on the oxygen sublattice;

O_{Cu} – antisite O atom on the copper sublattice;

Cu_{I6} – Cu atom in the 6-fold coordinated *octahedral* interstitial position;

O_{I6} – O atom in the 6-fold coordinated *octahedral* interstitial position;

Cu_{I4} – Cu atom in the 4-fold coordinated *tetrahedral* interstitial position;

O_{I4} – O atom in the 4-fold coordinated *tetrahedral* interstitial position.

To denote the charge state of a defect, we will use quasichemical notation of Kröger and Vink, where the symbol identifies the defect (an atom or a vacancy), its subscript denotes the defect location (sublattice or interstitial site, as specified above), and its superscript ($\times$, $'$, or $\bullet$) denotes the charge state (neutral, negatively charged, or positively charged, respectively). For example, a neutral copper vacancy is denoted as, $V_{Cu}^{\times}$ a negatively charged oxygen interstitial as O_{I4}', and a positively charged oxygen vacancy as $V_O^{\bullet}$. The electronic defects are denoted similarly as e' (conduction electron) and $h^{\bullet}$ (valence hole). The symbol $\varnothing$ ("empty set") is used to denote the absence of defects.

2.1 Diffusion and electrical conductivity data

Models of the defect structure of Cu_2O are mostly based on experimental data about the ionic diffusivity and electronic (hole) conductivity of this material, as functions of the oxygen partial pressure P_{O_2} and temperature T. The results of high-precision measurements of these transport properties of cuprite are available in Refs. Moore and Selikson (1951, 1952), Toth et al. (1961), O'Keeffe and Moore (1961, 1962), Tomlinson and Yates (1977), Maluenda et al. (1981a, b), Ochin et al. (1984, 1985), Timm and Janek (2005).

2.2 Nonstoichiometry in Tretyakov's model

Cuprite is a metal-deficient, *p*-type, extrinsic semiconductor whose properties are consistent with a structural model based on the presence of cation vacancies as the predominant ionic defects at sufficiently high temperatures and oxygen activities. Nonstoichiometry of cuprite was investigated by gas volumetric analysis (Dünwald and Wagner 1933), thermogravimetry (O'Keeffe and Moore 1962), and chemical analysis of quenched samples (Wagner and Hammen 1938). The data obtained at that time were very inconsistent. The range of homogeneity of cuprous oxide includes compositions from $Cu_{1.996}O$ to $Cu_{1.9994}O$ at 1,000°C (Dünwald and Wagner 1933), i.e. cuprous oxide in the equilibrium state is always metal deficient. According to the data of Wieder and Czanderna (1962) this deficit is larger and extends to the composition $Cu_{1.5}O$. In Bloem's opinion (Bloem 1958, Kröger 1964) the range of homogeneity of the cuprite phase also includes compositions with deficient oxygen (at low oxygen activities). The measurements of Müser and Schilling (1952) and Tretyakov et al. (1972) appear to corroborate this fact. The conclusions about the nature of the dominant defects are not uniform. The data obtained by Dünwald and Wagner (1933) are interpreted in terms of singly ionized copper vacancies and holes (Kröger 1964), whereas more recent results of McKinzie and O'Keeffe (1967), and those of Tretyakov et al. (1972), indicate neutral copper vacancies as predominant defects.

High-temperature (950–1,050°C) electrochemical measurements (coulometric titration) performed by Tretyakov et al. (1972) gave the following relations for the nonstoichiometry γ of cuprite $Cu_2O_{1+\gamma}$ as a function of oxygen pressure P_{O_2} (the energies are in calories per mole):

a. high-P_{O_2} range (1–30 torr)

$$\gamma = 2.9 \cdot \exp\left(-\frac{17500 \pm 4700}{RT}\right) \cdot P_{O_2}^{1/4} \tag{2-1}$$

b. low-P_{O_2} range (10^{-3}–1 torr)

$$\gamma = -4.32 \cdot 10^4 \cdot \exp\left(-\frac{54700 \pm 8000}{RT}\right) \cdot P_{O_2}^{-1/2} \tag{2-2}$$

In combination with other experimental data, the knowledge of parameter *n* that enters expressions like $\gamma = K \cdot P_{O_2}^{1/n}$ allows one to determine the predominant type of atomic defect, as well as its state of ionization. As follows from theory of disorder (Kröger 1964), value $n = 4$ in Eq. (2-1) is compatible with the following quasichemical reactions of defect formation:

$$\tfrac{1}{2}O_2 \rightarrow O_O^{\times} + 2V_{Cu}^{\times} \tag{2-3}$$

or

$$\tfrac{1}{2}O_2 \rightarrow O_I' + h^{\bullet} \tag{2-4}$$

Here the quasichemical notation of Kröger is used, where the superscript gives the charge state of a defect (crosses, primes, and dots representing neutral, negative, and positive charges, respectively)[3].

Tretyakov et al. (1972) argue that since cuprous oxide is characterized by large deviations from stoichiometry (up to $\gamma \cong 10^{-3}$ at 1,000°C), the experimental data favor neutral copper vacancies as the predominant defects in the lattice for the high-P_{O_2} range. According to Tretyakov et al. (1972), large deviations from stoichiometry according to Eq. (2-4) are unlikely, due to crystal-chemistry considerations.

[3] Most likely, the interstitial oxygen that forms as a result of reaction (2-4) occupies a tetrahedral interstitial position, i.e. O_{I4}'. In our calculations its energy is found to be lower than that of an oxygen ion in the octahedral interstitial position.

For the low-P_{O_2} range of stability of cuprite, Eq. (2-2) gives $n = -2$, which is consistent with the following quasichemical reaction[4]:

$$O_O^\times \rightarrow \tfrac{1}{2}O_2 + V_O^\times \qquad (2\text{-}5)$$

From Eqs. (2-1) and (2-2) one finds the energies of formation for (neutral) copper and oxygen vacancies, respectively:

$H(V_{Cu}^\times) = 17.5 \pm 4.7$ kcal·mol^{-1} (0.76 eV) and

$H(V_O^\times) = 54.7 \pm 8.0$ kcal·mol^{-1} (2.37 eV)

From these values, the enthalpy of formation of a Schottky defect,

$$\varnothing \rightarrow V_O^\times + 2\,V_{Cu}^\times \qquad (2\text{-}6)$$

can be deduced, $H_S = 89.6 \pm 13.4$ kcal/mole (3.9 ± 0.6 eV). This value is in good agreement with $H_S = 91$ kcal·mol^{-1} (3.95 eV) obtained by Bloem (Bloem 1958, Kröger 1964) through analysis of the optical spectrum of cuprous oxide.

However, the defect model proposed for non-stoichiometric cuprite by Bloem (1958) is quite different from the model put forward by Tretyakov et al. (1972). Bloem's model has been analyzed in detail by Kröger (1964) and will be considered in Section 2.3. Let us note here that in Bloem's model, the deviation from stoichiometry in cuprite, at high temperatures, is formed by *charged* defects, according to the following quasichemical reactions:

$$\tfrac{1}{2}O_2 \rightarrow O_O^\times + 2V_{Cu}' + 2h^\bullet \qquad (2\text{-}7)$$

for copper-deficient cuprite (high-P_{O_2} range) and

$$O_O^\times \rightarrow \tfrac{1}{2}O_2 + 2V_{Cu}' + 2V_O^\bullet \qquad (2\text{-}8)$$

for copper-rich cuprite (low-P_{O_2} range).

2.3 Thermal disorder in Bloem's model

Bloem (1958) has proposed a model based on Schottky type of disorder in cuprite. The model is based on the experimentally observed isotherms of electrical conductivity as a function of oxygen pressure, $\sigma \propto P_{O_2}^{1/n}$, which show rather high absolute values of n, ranging between 3 and 8, depending on the temperature. The main equations and energies in Bloem's model are as follows:

$$\varnothing \rightarrow e' + h^\bullet \qquad E_i = 2.15 - 5\cdot10^{-4}\cdot T\,[\mathrm{K}]\ \mathrm{eV}; \qquad (2\text{-}9)$$

$$\varnothing \rightarrow 2V_{Cu}^\times + V_O^\times \qquad H_S = 3.95\ \mathrm{eV}; \qquad (2\text{-}10)$$

$$V_{Cu}^\times \rightarrow V_{Cu}' + h^\bullet \qquad E_a = 0.5\ \mathrm{eV}; \qquad (2\text{-}11)$$

$$V_O^\times \rightarrow V_O^\bullet + e' \qquad E_b = 0.3\ \mathrm{eV}; \qquad (2\text{-}12)$$

$$V_O^\bullet \rightarrow V_O^{\bullet\bullet} + e' \qquad E_{b2} = 1.2\ \mathrm{eV}\ (1{,}000°\mathrm{C}),\ E_{b2} = 1.35\ \mathrm{eV}\ (700°\mathrm{C}); \qquad (2\text{-}13)$$

$$V_{Cu}' + V_O^\bullet \rightarrow (V_{Cu}V_O)^\times \qquad H_P = -0.5\ \mathrm{eV}. \qquad (2\text{-}14)$$

[4] In this case, the formation of associated interstitial copper ions, for example, $2Cu_{Cu}^\times + O_O^\times \rightarrow \tfrac{1}{2}O_2 + (Cu_{I6})_2^\times$ is disregarded. This conclusion of Tretyakov et al. (1972) agrees with the results of our *ab initio* calculations, as will be discussed later in this Section.

Bloem's model seems to give a fair description of the observed $\sigma(P_{O_2})$ isotherms, however, Kröger has pointed out several internal inconsistencies in the model and concluded that the model may be wrong in one or more essential points. More recent experimental data (McKinzie and O'Keeffe 1967, Tretyakov et al. 1972) have also cast some doubts on the validity of Bloem's model. Let us, however, review the main conclusions that can be derived from that model, since they are of direct interest.

1. The deviation from stoichiometry in cuprite at high temperatures is formed according to defect reactions Eqs. (2-7) and (2-8), i.e. by charged vacancies. The electrical neutrality conditions for the copper-deficient and copper-rich regions are, respectively,

   $$p = [V'_{Cu}] \tag{2-15}$$

   and

   $$[V^{\bullet}_{O}] = [V'_{Cu}] \tag{2-16}$$

   Here $p \equiv [h^{\bullet}]$ denotes the concentration of holes; by square brackets we denote the concentration (number of defects per unit volume) of the defect species specified in the brackets. In the copper-rich region, where $[V^{\bullet}_{O}] = [V'_{Cu}]$, the model predicts that the concentration of copper vacancies must increase with increasing the deviation from stoichiometry, contrary to what one would expect. Kröger points out that a similar situation has actually been observed in BaO. The fact that Bloem's model predicts the concentration of copper vacancies to be a minimum near the stoichiometric point may have important implications for self-diffusion in cuprite, which is mediated by copper vacancies. Thus, cation diffusion through the oxide film is found to be the rate-controlling process in copper corrosion (Feng et al. 1996a, b).

2. According to the model, most oxygen vacancies in cuprite are present in a singly ionized charge state, $V^{\bullet}_{O}$. It follows from the model that a single ionization is possible, because $E_i > E_a + E_b$; however, the band gap in cuprite is not large enough to produce doubly ionized oxygen vacancies, that is, $E_i < 2E_a + E_b + E_{b2}$. According to this, at the stoichiometric composition where $[V'_{Cu}] + [V^{\times}_{Cu}] = 2[V^{\bullet}_{O}]$ and where the two dependencies given by Eqs. (2-15) and (2-16) meet each other, one finds an uncompensated p-density, $p > n$, which means that stoichiometric Cu_2O is an intrinsic p-type semiconductor. This result has been referred to in Section 1.2.

2.4 Defect structure model by Peterson and Wiley

Peterson and Wiley (1984a, b) made an experimental study of diffusion and point defects in Cu_2O as a function of temperature (700–1,153°C) and oxygen partial pressure (10^{-6}–$8 \cdot 10^{-2}$ atm). The authors find that both neutral and singly charged copper vacancies contribute to cation self-diffusion. The authors develop a simple model involving such defects as copper vacancies, electron holes, and singly-charged oxygen interstitial ions, and fit the model to experimental tracer-diffusion and electrical conductivity data (Maluenda et al. 1981b), as well as to the equilibrium stoichiometry data (O'Keeffe and Moore 1961). According to the model, the predominant defect type in cuprite is a neutral cation vacancy, Eq. (2-3), which may become singly charged:

$$V^{\times}_{Cu} \rightarrow V'_{Cu} + h^{\bullet} \tag{2-17}$$

The formation of singly charged oxygen interstitials O'_I is described by reaction Eq. (2-4). The resulting defect model was found to be qualitatively consistent with the diffusion data of Maluenda et al. (1981a), to which the model had not been fitted.

2.5 Defect structure model by Xue and Dieckmann

Xue and Dieckmann (1990) developed their model on the basis of their own thermogravimetric data as a function of oxygen activity at temperatures between 800 and 1,200°C, in combination with the literature data on cation diffusion, anion diffusion, and electrical conductivity. The model was set up to be quite flexible before fitting it to the data; it included four defects (two vacancies and two interstitials), thus allowing for the Schottky type of disorder, as well as for the cation and anion Frenkel type of disorder.

Neutral copper vacancy $V_{Cu}^{\times}$ and neutral oxygen vacancy $V_O^{\times}$ have been identified to be the dominant defects at high and low oxygen activity, respectively. Neutral oxygen interstitials $O_I^{\times}$, singly charged copper vacancies V'_{Cu}, and holes $h^{\bullet}$ have been identified to be important minority defects in $Cu_{2-\delta}O$. Fitting to the experimental data yielded a formation energy of 74.1 kJ·mol^{-1} (0.77 eV) for a neutral copper vacancy and 294.4 kJ·mol^{-1} (3.05 eV) for a neutral oxygen vacancy. Thus, the formation energy of a neutral Schottky defect is estimated as 442.6 kJ·mol^{-1} (4.6 eV), which is greater than the corresponding energies in Bloem's and Tretyakov's models.

2.6 Mobile charged defects in the model by Park and Natesan

Park and Natesan (1993) studied thermogravimetric copper oxidation in air and oxygen at temperatures between 300 and 1,000°C. Electronic transport in the so obtained non-stoichiometric copper oxides was studied as a function of temperature (350–1,134°C) and oxygen pressure (10^{-8}–1.0 atm). The measurements have indicated intrinsic electronic conduction in CuO over the entire range of condition, whereas in Cu_2O conduction was found to occur by means of doubly-ionized oxygen interstitials and holes. Calculated values of the enthalpy of formation of (interstitial) oxygen and the hole conduction energy have been estimated to be 2.0±0.2 eV and 0.82±0.02 eV, respectively.

2.7 Defect structure model by Porat and Riess

Porat and Riess (1994) performed comprehensive studies of non-stoichiometry, phase width, and dominant point defects in $Cu_{2-y}O$. The deviation from stoichiometry y was measured as a function of oxygen partial pressure ($10^{-13} \leq P_{O_2} \leq 0.1$ atm) and temperature ($873 \leq T \leq 1{,}245$ K) using a solid state electrochemical method. The obtained y–P_{O_2}–T relations have been analyzed in order to identify the dominant point defects. It has been found that in the high-P_{O_2} range, the dominant defects are neutral copper vacancies, $V_{Cu}^{\times}$. In the low-P_{O_2} range there are two types of defects, dominating at different temperatures. At low temperatures the dominant defects are neutral copper interstitials, $Cu_I^{\times}$. However, at temperatures higher than 1,245 K the dominant defects are found to be oxygen vacancies, $V_O^{\times}$. The enthalpy for the formation of $V_{Cu}^{\times}$ is found to vary from 60.2 kJ·mol^{-1} (0.62 eV) at 1,200 K to 37.6 kJ·mol^{-1} (0.39 eV) at 950 K. The former value (upper bound) is lower than the values obtained in all previous studies (Bloem 1958, Tretyakov et al. 1972, Peterson and Wiley 1984a, Xue and Dieckmann 1990). The enthalpy for the formation of $Cu_I^{\times}$ was found to be equal to 186 kJ·mol^{-1} (1.92 eV), independent of temperature.

In a subsequent study (Porat and Riess 1995) the transport properties of Cu_2O were measured as a function of temperature ($900 \leq T \leq 1{,}300$ K) and oxygen pressure ($10^{-12} \leq P_{O_2} \leq 0.15$ atm), to identify that the dominant charge carriers were holes, although at high temperatures (above 1,200 K) and low oxygen partial pressure (below 10^{-5} atm) there was a significant contribution of electrons to the electrical conductivity and Seebeck coefficient. The dominant ionic point defects were identified as doubly charged oxygen interstitials, O_I'', at temperatures above 1,150 K, and singly charged copper vacancies V'_{Cu}, at temperatures below 950 K.

By fitting the appropriate models to the experimental data, the authors found the hole and electron mobilities at temperatures of $1{,}000 \leq T \leq 1{,}250$ K. The hole mobility decreases with increasing temperature, with values in the interval $3 \leq v_h \leq 6$ cm^2·V^{-1}s^{-1} for temperatures $1{,}250 \geq T \geq 1{,}000$ K, respectively. These values are found to be in agreement with data extrapolated from low temperatures. The electron mobility was found to be almost temperature independent, with values of $150 \leq v_e \leq 200$ cm^2·V^{-1}s^{-1} at similar temperatures.

The enthalpies and entropies for the formation of O_I'' and V'_{Cu} were also determined. For the enthalpy and energy of a defect reaction,

$$\tfrac{1}{4}O_2 \rightarrow \tfrac{1}{2}O_O^{\times} + V'_{Cu} + h^{\bullet},$$

one gets $\Delta H = 1.8 \pm 0.2$ eV and $\Delta S = (9 \pm 0.11) \cdot 10^{-3}$ eV·K^{-1}.

For the reaction

$\frac{1}{2}O_2 \rightarrow O_I'' + 2h^\bullet$

the result is $\Delta H = 3.1 \pm 0.1$ eV and $\Delta S = (14 \pm 0.2) \cdot 10^{-3}$ eV·K^{-1}.

2.8 Other defect models of cuprite

The defect structure of Cu_2O is still the subject of scientific debate. The Reader is referred to recent publications (Haugsrud and Kofstad 1997, Dieckmann 1998, Tsur and Riess 1998, 1999, Haugsrud and Norby 1999, Rosenstock and Riess 2000, Haugsrud 2002, Zhu et al. 2004) in which other empirically-based models and aspects of the defect structure of cuprite are discussed. Defect structure models of Cu_2O have also been derived from first-principles electronic-structure calculations by Raebiger et al. (2007) and Scanlon and Watson (2011), they will be reviewed in the following subsections.

2.9 Present *ab initio* calculations

In the present work an attempt has been made to calculate the defect formation energies in cuprite using a supercell approach and the KKR-ASA+M method within the locally self-consistent Green's function (LSGF)formalism. The details of our electronic structure calculations were as follows. The supercells were obtained by 2×2×2 multiplication of the cuprite unit cell. Each supercell contained 32 atomic positions for Cu, 16 atomic positions for O, and 80 empty spheres (totally 128 lattice sites). The calculations were performed for all possible kinds of point defects in Cu_2O (one defect per supercell, neutral state): vacancies V_{Cu} and V_O; antisites Cu_O and O_{Cu}; and atoms in the tetrahedral (I4) and octahedral (I6) interstitial positions, Cu_{I4}, O_{I4}, Cu_{I6}, and O_{I6}. Some defect complexes, like (V_{Cu} V_O), were also considered. To perform electronic structure calculations for the corresponding supercells, we employed an order-*N*, locally self-consistent Green's function (LSGF) method of Abrikosov et al. (1997), in which the computational time scales only linearly with the number of atoms. The local interaction zone (LIZ), in which the multiple-scattering problem was solved exactly, contained up to eight coordination shells of atoms and empty spheres around each site of the supercell. The rest of the parameters of our KKR-ASA+M calculations were identical to those listed in Section 1.3.

The ASA+M scheme (Korzhavyi et al. 1999, 2000) allows one to take into account non-spherical (multipole) moments of the electron charge density, but it does not permit for structural (local) relaxation around point defects. Therefore, in the KKR-ASA+M calculations we took into account only the global, volume relaxation of the supercells, whereas all the atoms were considered to be located at their ideal lattice positions. The effect of lattice strain on defect energetics in metals (Korzhavyi et al. 1999), intermetallic compounds (Korzhavyi et al. 2000, 2002a, Hugosson et al. 2001), and even in some semiconductors (Korzhavyi et al. 2002b) is often found to be relatively small (as compared to the band gap error, for example), so that our neglect of lattice relaxations does not affect these results qualitatively.

Previously, density functional theory was used to examine aspects of the copper vacancy (V_{Cu}) in cuprous oxide (Wright and Nelson 2002). The normal vacancy configuration, obtained by a simple removal of a Cu atom from the lattice, is found to be 0.1 eV higher in energy than a split vacancy configuration wherein a nearby Cu atom is displaced toward a normal vacancy site by half the bulk Cu-Cu separation. Jumps between the normal and split vacancy configurations are predicted to be rate limiting for the V_{Cu}-mediated diffusion with an energy barrier of 0.3 eV.

The main results of the present investigation are shown in Figure 2-1 and Table 2-1. Figure 2-1 shows the calculated heat of formation of stoichiometric Cu_2O and of eight nonstoichiometric supercells, each containing one of the eight possible (neutral) defects in cuprite. On either side away from the stoichiometric composition there are four branches of the heat of formation as a function of composition, each branch corresponds to a certain defect responsible for the departure from stoichiometry. The lowest branch on each side corresponds to the constitutional defect, i.e. the dominant defect in the limit $T \rightarrow 0$.

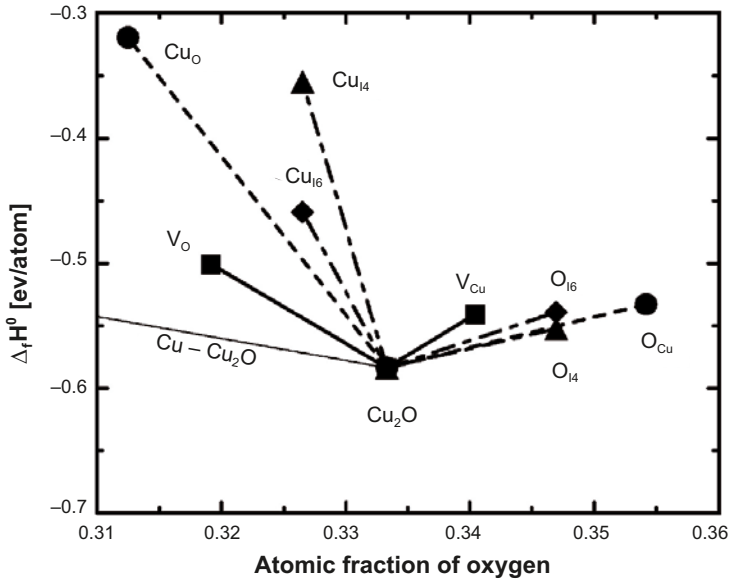

Figure 2-1. *Calculated heats of formation (shown as symbols) for the stoichiometric cuprite and nonstoichiometric, charge-neutral supercells each containing one of the eight possible types of point defects in Cu_2O. Branches of the heat of formation as a function of composition are shown as lines. The thin line connects pure Cu and Cu_2O.*

Table 2-1. *Ab initio* calculated and experimental formation energies [eV] of neutral point defects in Cu_2O. The energies are expressed relative to Cu_2O-O_2 chemical potential (Cu-poor–O-rich compositions).

	V_O	Cu_O	Cu_{I6}	Cu_{I4}	V_{Cu}	O_{Cu}	O_{I6}	O_{I4}
Theory [a] (unrelaxed)	3.8	14.3	4.5	13.2	0.6	1.7	2.1	0.3
Theory [b]	1.4		2.7	2.8	1.0		1.7	1.5
Experiment [c]	2.4				0.8			
Experiment [d]	3.1				0.8			
Experiment [e]			1.9		0.4–0.6			

[a] KKR-ASA+M (unrelaxed geometry), this work.

[b] VASP-PAW & Hybrid functional (Scanlon and Watson 2011).

[c] Tretyakov et al. (1972).

[d] Xue and Dieckmann (1990).

[e] Porat and Riess (1994).

On the copper-rich side, our calculations predict that neutral oxygen vacancies are the constitutional defects. This conclusion is in agreement with the result obtained by Tretyakov et al. for the low-P_{O_2} range. We have also performed calculations in which a pair of nearest-neighbor vacancies (V_{Cu} V_O) was considered, which must be the dominant defect pair in this region of compositions according to Bloem. However, we find that the formation energy of this defect pair is nearly equal to that of a copper atom in the octahedral interstitial position, Cu_{I6}, so that the corresponding branch lies much higher than the branch due to neutral oxygen vacancies.

For copper-deficient compositions, our calculations predict the oxygen interstitial atom, O_{I4}, to be the lowest-energy defect. The possibility of formation of this defect was disregarded by Tretyakov et al. (1972) on the basis of crystal chemistry considerations. Copper vacancies, which are considered to be the dominant defects in copper-deficient cuprite at high temperatures, are found to be higher in energy than additional oxygen atoms in tetrahedral interstitial positions at zero temperature. There may be two sources of this discrepancy between theoretical and experimental results. First of all, as Table 2-1 shows, the calculated (unrelaxed) values of the vacancy formation energies are some 1 eV

higher than the corresponding data obtained by Tretyakov et al. (1972). Secondly, in compounds one often meets the situation when higher-energy defects become dominant at high temperatures due to their higher formation *entropy* (Korzhavyi et al. 2000). These so-called interbranch defects, which become more stable at high temperatures than the low-energy defects, may occur very easily, especially if the energy difference between the two kinds of defects is small.

2.10 Nature of *p*-type conductivity of Cu_2O

Let us now review some experimental data on the electrical properties of Cu_2O that may be useful for electrochemical calculations. Kröger (1964) reports on the following high-temperature data concerning the activation energy for electronic (*p*-type) conductivity in cuprite: The activation energy varies from 1.06 eV at $P_{O_2} < 10^{-2}$ mm Hg, via 0.65 eV for $10^{-2} < P_{O_2}$ 10 mm Hg, to 0.77 eV at 150 mm Hg, and ≅ 1 eV at 1 atm. (Piippo et al. 1998) have studied the electric properties of anodically formed oxide films on Cu. For Cu_2O films they deduced a value of 12 for the dielectric constant, values of $1.4–7 \cdot 10^{20}$ cm^{-3} for the acceptor density, and a value of about 50 $kJ \cdot mol^{-1}$ (0.51 eV) for the activation energy.

Nolan and Elliott (2006) have investigated the origin of *p*-type conduction and its mechanism in Cu_2O using first-principles calculations. Plane wave density functional theory (DFT) with the Perdew-Burke-Ernzerhof (PBE) exchange-correlation functional is applied. In order to investigate the applicability of DFT, Nolan and Elliott (2006) firstly show that CuO, with 50% Cu vacancies, cannot be described with DFT and, in order to obtain a consistent description of CuO, the DFT+*U* approach is applied. The resulting electronic structure is consistent with experiment, with a spin moment of 0.64 μ_B and an indirect band gap of 1.48 eV for $U = 7$ eV. However, for a 3% Cu vacancy concentration in Cu_2O, the DFT and DFT+*U* descriptions of Cu vacancies are similar, indicating that DFT is suitable for a small concentration of Cu vacancies; the formation energy of a Cu vacancy is no larger than 1.7 eV. Formation of Cu vacancies is found to produce delocalized hole states with hole effective masses consistent with the semiconducting nature of Cu_2O. Thus, the authors attribute the *p*-type semiconducting properties observed for Cu_2O to a small concentration of Cu vacancies.

Raebiger et al. (2007) have investigated the origins of the *p*-type nature and cation deficiency in Cu_2O and related materials. The authors employ first-principles techniques to calculate formation energies for various intrinsic defects and their ionization energies, as well as defect and carrier concentrations. Their calculations employ the generalized gradient approximation (GGA) to density-functional theory using the projector augmented-wave method as implemented in the VASP code. The defects are simulated using supercells with 96 Cu_2O lattice sites, including a single lattice defect in various charge states. A fixed, GGA-calculated of the lattice constant for Cu_2O, 4.313 Å, is used; all atomic positions are allowed to relax.

Raebiger et al. (2007) have shown from the first principles calculations that Cu_2O is intrinsically copper-deficient due to formation of copper vacancies V_{Cu} that act as a shallow and efficient hole producers. Cu_2O is intrinsically *p*-type because (i) the potential hole killer V_O has no transition level in the gap and thus cannot annihilate holes, and (ii) the possible hole killer Cu_{I6} has both high formation energy and deep transition level and is thus incapable to efficiently destroy holes created by V_{Cu}. The rule for *p*-type oxide design is that the valence band maximum should be formed by the interaction between a filled anion shell and a filled cation shell that lie as high in energy as possible. Suitable cations apart from Cu(d^{10}) would thus be, e.g. Ag(d^{10}) and Au(d^{10}), as well as, e.g. elements from group VIII (Co, Rh, Ir) in the d^6 low-spin state.

Although the approaches employed by authors of Refs. Nolan and Elliott (2006) and Raebiger et al. (2007) are very similar to each other, the conclusions differ quite significantly. One should probably trust the conclusions derived by Raebiger et al. (2007) since these authors have considered a rich defect structure. Also, their conclusions are similar to those of the most comprehensive experimental studies (Porat and Riess 1994, 1995).

2.11 Hydrogen in cuprite

There are two even more recent studies concerned with the defect structure calculations of Cu_2O in which the possible role of hydrogen has been addressed (Wang et al. 2010, Scanlon and Watson 2011). Wang et al. (2010) have performed a computational study into the effect of pH on the defect structure and transport properties of cuprite, assuming that it is synthesized from an aqueous solution. Scanlon and Watson (2011) have analysed the various interstitial sites of H residence in cuprite and found that hydrogen forms a strongly bound complex with a copper vacancy. Moreover, the hydrogen is found to prefer not to occupy the center of the vacancy, but to move away from the center closer to one of the two oxygen anions. This geometry of the V_{Cu}-H defect cluster is reminiscent of the hydrogen position in the structure of cuprous hydroxide obtained in our recent *ab initio* studies (Korzhavyi and Johansson 2010, Korzhavyi et al. 2011). This structural similarity allows for the interpretation of unsymmetric hydrogen position inside a copper vacancy in cuprite as the formation of a hydroxyl (OH) group connected to the other neighbouring oxygen anion by a hydrogen bond.

3 Initial stages of copper oxidation

Numerous experimental studies of adsorbed oxygen on metal surfaces have been performed, with the main attention paid to reactivity of the adsorbed oxygen, which is of interest for heterogeneous catalysis. The obtained data on the structure that forms at the initial stages of oxidation, as well as on the kinetics of the oxidation process, represent great interest for much broader range of applications. In this chapter, the data relevant to the process of copper corrosion will be presented.

In Figure 3-1 we introduce the notations for selected surface adatom positions (a–c) and surface reconstruction patterns (d–f) at the low-index Cu surfaces, (100), (110), and (111). The notations are similar to those used by Rous (1995). Typical adsorbed layer structures formed on surfaces of selected transition and noble metals, investigated up to year 1995, are reviewed in Rous (1995).

3.1.1 Cu(100) surface

Since Lee and Farnsworth (1965) observed a faint four-spot LEED pattern on an oxygen adsorbed Cu(100) surface, many investigators have argued for more than 30 years about the adsorbed oxygen on the Cu(100) surface whether it forms a long-range ordered $c(2\times2)$-O structure or not (Simmons et al. 1967, Oustry et al. 1973, McDonnell and Woodruff 1974). The only structure with long-range order is found to be the reconstructed $(2\sqrt{2}\times\sqrt{2})$R45°-O structure with the saturation coverage of 0.5 ML (monolayer) (Jensen et al. 1990).

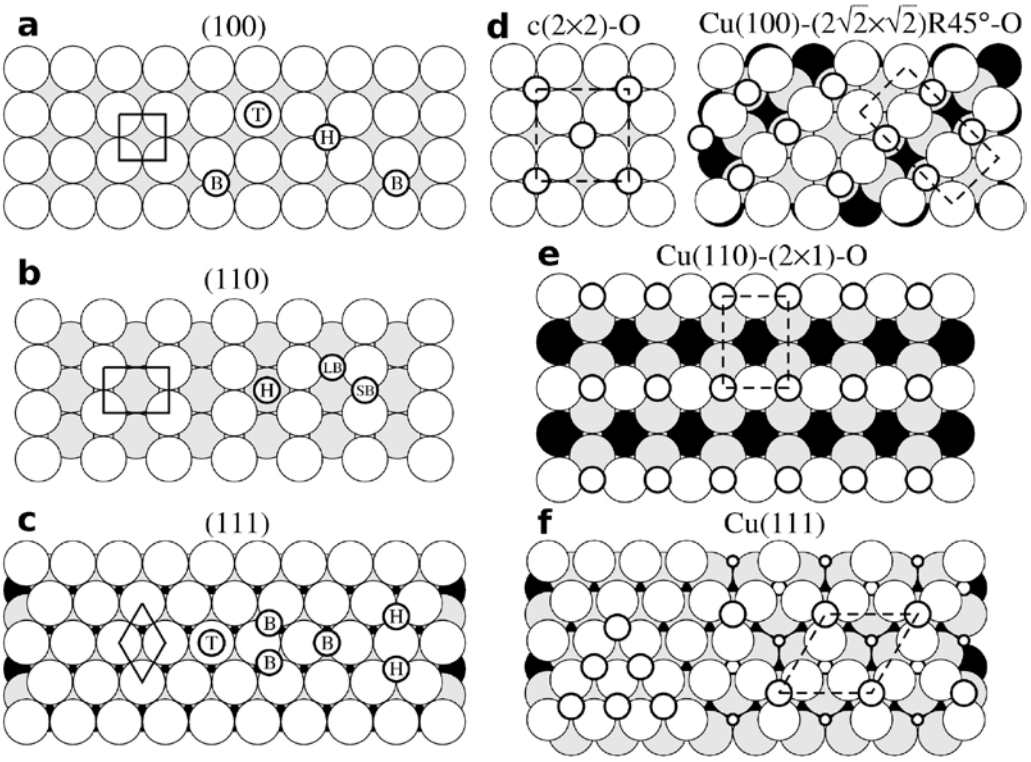

Figure 3-1. *Top view of the fcc (100), (110), and (111) surfaces showing possible high-symmetry adsorption sites (a–c) and typical surface reconstruction patterns (d–f) induced by oxidation. Large circles indicate copper atoms; atoms in the topmost layer are white, in the second layer–gray, and in the third layer–black. Oxygen atoms are shown as smaller circles with bold outline; in (f) their size decreases as the oxygen atoms go deeper into the surface. The surface unit cell for the unreconstructed(reconstructed) surfaces is indicated by continuous(broken) bold lines. The notations for adsorption sites are as follows: B: bridge site, LB: long-bridge site, SB: short-bridge site, T: top site. On the (100) and (110) surfaces H denotes the four-fold and two-fold hollow sites, respectively. There are two possible three-fold hollow sites on the (111) surface, the fcc-hollow or the hcp-hollow (hexagonal close-packed).*

The dissociative adsorption of oxygen molecules to clean Cu(100) surface have been investigated in detail relatively recently (Spitzer and Lüth 1982a, Katayama et al. 2007, Yagyu et al. 2007, 2009). Fujita et al. (1996) have solved the atomic structure that forms on the Cu(100) surface at low values of oxygen coverage. Further structural studies, at low and high coverage values, have been performed (Kittel et al. 2001). They find that adsorbed oxygen atoms exclusively occupy four-fold hollow sites on Cu(100), but a continuous $c(2\times2)$-O structure Figure 3-1(d) does not form. The actual structure has been found to consist of nano-sized $c(2\times2)$-O ordered domains separated by oxygen-deficient antiphase boundaries. The boundaries are zig-zag shaped and their density reaches a maximum at $\Theta \cong 0.3$ ML. The reason for the development of such a structure with nano-sized domains is that it disperses the stress accumulated on the surface upon oxygen adsorption (Harrison et al. 2006): The density of Cu atoms in fcc Cu is too high compared to that in Cu_2O.

Tanaka et al. (1998) have found that a large $c(2\times2)$-O domain is transitively formed when the oxygen coverage exceeds a critical value of 0.3 ML. The large domain forms by coalescence of nano-sized $c(2\times2)$-O domains by the following mechanism. First, oxygen is adsorbed at the antiphase boundary separating two small domains. Then all the oxygen atoms of one of the two small domains instantaneously migrate as a two-dimensional domino fall.

Large $c(2\times2)$-O domains are unstable structures, since they accumulate high stress. This stress is the driving force towards a missing-row type surface reconstruction into the stable $(2\sqrt{2}\times\sqrt{2})$R45°-O structure, which can be viewed as a $c(2\times2)$-O structure with each fourth [001] row of Cu atoms missing, see Figure 3-1(d). Tanaka et al. (1998) find that the reconstruction occurs by emission of Cu atoms from the large $c(2\times2)$-O domains.

The emitted Cu atoms are not trapped at the surface steps, but form islands on terraces. The islands take the stable $(2\sqrt{2}\times\sqrt{2})$R45°-O structure with one atom height. Taking into account the fact that oxygen coverage is 0.5 ML on the islands while it is 0.3 ML on the terrace, growth of Cu islands consumes the oxygen on the terrace so that remaining nano-sized $c(2\times2)$-O domains change to a clean surface area.

The effective-medium theory was employed by Jacobsen and Nørskov to study oxygen-induced reconstruction of Cu(110) and Cu(100) surfaces (Jacobsen and Nørskov 1990). In their model calculation they obtained the structures and energetics of the reconstructed as well as of unreconstructed surfaces. The equilibrium chemisorption energies (relative to atomic oxygen and a clean unreconstructed surface) for the Cu(100) were found to be −10.50 and –9.38 eV for the missing-row reconstructed $(2\sqrt{2}\times\sqrt{2})$R45°-O and unreconstructed $c(2\times2)$-O structures, respectively. Therefore, the energy gained upon reconstruction was found to be 1.12 eV. The calculated bond lengths and vibrational frequencies for the reconstructed surfaces were found to be in good agreement with experiment.

Since surface diffusion of copper is involved in the process of $(2\sqrt{2}\times\sqrt{2})$R45°-O surface reconstruction, some information on the copper mobility on Cu(100) is of interest. The activation energy of 0.36−0.40 eV for Cu adatom diffusion on Cu(100) surface has been reported (De Miguel et al. 1987, Breeman and Boerma 1992, Dürr et al. 1995). Diffusion of Cu within the surface layer occurs by vacancy mechanism. The formation and migration energies of 0.51 eV and 0.29 eV, respectively, for a vacancy on Cu(100) have been calculated using the embedded atom method (EAM) (van Gastel et al. 2001). Scanning tunneling microscopy study of In atoms migration on the Cu(100) surface has yielded an estimate of the self-diffusion coefficient for copper terrace atoms, $D = 0.42$ Å^{2}s^{-1} at 320 K (van Gastel et al. 2001).

Homoepitaxial growth of Cu(100) surface pre-exposed to oxygen was studied by Yata et al. (1997). The pre-exposed surface had a $(2\sqrt{2}\times\sqrt{2})$R45°-O structure, see Figure 3-1(d). Upon deposition of copper on top of the adsorbed oxygen layer, the buried oxygen atoms segregated to the surface layer, to retain the energetically more favorable missing-row reconstructed surface. The activation energy for the process of the oxygen transport from under the deposited copper layer to the surface layer was estimated as 0.66 eV.

An up-to-date summary of experimental and theoretical activities concerning oxidation of Cu(100) surface in controlled oxygen atmosphere can be found in Lahtonen et al. (2008). The same reference also contains the results of an original STM investigation of all stages of the oxidation process, from oxygen adsorption to oxide formation.

3.1.2 Cu(115) and Cu(119) surfaces

Being exposed to oxygen, high-index surfaces of Cu undergo faceting. Both the Cu(115) and Cu(119) surfaces reconstruct into two kinds of {104}-type facets and a third facet determined by the macroscopic surface orientation. This third facet is {113}-oriented for Cu(115) and {100}-oriented for Cu(119) (Reinecke and Taglauer 2000). On all facets …Cu-O-Cu-O… chains are developed that are energetically favored. The energetics of Cu(115) faceting has been studied by Walko and Robinson (2001) and Chaika et al. (2008).

On oxygen-saturated surfaces the facet size is determined by the formation kinetics. The facet size dependence on sample temperature or oxygen pressure can be formally described by the nucleation and growth mechanism. The activation energy of faceting has been estimated as 0.21±0.01 eV (Reinecke and Taglauer 2000).

3.1.3 Cu(110) surface

Oxygen adsorbed to Cu(110) surface is also found to induce a missing-row reconstruction of the surface, to form a (2×1)-O structure with the oxygen coverage of 0.5 ML (Besenbacher and Nørskov 1993). Another type of surface reconstruction, *c*(6×2)-O has also been reported (Ertl 1967, Kishimoto et al. 2008). A recent STM study (Coulman et al. 1990) has revealed that the mechanism for the formation of the (2×1)-O phase is the condensation of mobile chemisorbed O atoms with Cu adatoms which leave from step edges and diffuse across the terraces, see also Sun et al. (2007) and Brandstetter et al. (2008). Because of strongly attractive Cu-O interactions, long …Cu-O-Cu-O… strings are formed along the [001] direction on top of the substrate. These strings act as nuclei for the reconstructed phase, which for oxygen coverage lower than $\Theta = 0.5$ ML, consist of highly anisotropic islands (stripes) having an added-row structure (Besenbacher and Nørskov 1993, Coulman et al. 1990, Zhou and Yang 2003, Blanchard et al. 2005).

For a wide coverage range, $0.05 < \Theta < 0.45$, of the Cu(110) surface the Cu-O island stripes consist of 8–14 virtually infinite …Cu-O-Cu-O… rows; the stripes remarkably self-organize in a periodic array (called a supergrating) with a spacing varying between 60 and 140 Å. The dependence of the period of the super-grating as a function of oxygen coverage has been explained (Vanderbilt 1992, Zeppenfeld et al. 1994) in terms of effective long-range interactions decaying as l/r^2. Most likely, these interactions are of elastic type (Berge and Goldmann 2003, Prévot et al. 2004, Bobrov and Guillemot 2008) and originate from the mismatch between the preferred period of the …Cu-O-Cu-O… strings and the period of the Cu(110) substrate in the [001] direction. Thus, buckling of the …Cu-O-Cu-O… strings has been observed (Mocuta et al. 1999). The displacements of atoms are relatively small, less than 0.1 Å. Oxidized Cu(110) surface is considerably more ordered than Cu(100) (Bobrov and Guillemot 2008) and also shows a highly enhanced oxidation rate in the initial stage of oxidation (Zhou and Yang 2003).

Jacobsen and Nørskov (1990) calculated the equilibrium chemisorption energy to be −10.57 eV for the (2×1)-O reconstructed Cu(110) surface, and −10.13 eV for the unreconstructed surface with the oxygen atoms occupying the long-bridge sites. The net energy gain due to reconstruction is 0.44 eV[5]. The activation energy of the growth of the organized …Cu-O-Cu-O… chains has been experimentally measured and found to be of 0.22±0.01 eV, a very small value. The very low activation barrier compares well with the low energy barriers for Cu and O diffusion found in a first-principles calculation study (Liem et al. 1998). Liem et al. (1998, 2000) used first-principles calculations to model the adsorption and dissociation of oxygen on the Cu(110) surface. They found that an oxygen atom on a clean, unreconstructed Cu(110) surface is most stable in a position close to the four-fold hollow site (at low oxygen coverage of $\Theta = 1/6$). At half-coverage, the most stable structure is found to be the (2×1)-O pairing row reconstructed structure, in agreement with experiment. The diffusion barriers for O and Cu atoms have been calculated and found to be: 0.15 eV and 0.30 eV for O diffusion in the $[1\bar{1}0]$ and [001] directions, respectively, and 0.35 eV and 0.23 eV for Cu diffusion in the $[1\bar{1}0]$ and [001] directions, respectively.

[5] The cost in energy to make a missing-row reconstruction is 0.30 eV for both Cu(100) and Cu(110) clean surfaces (for both surfaces the value refers to two primitive cells of the unreconstructed surface).

3.1.4 Cu(111) surface

Pure (111) surface is almost non-reactive relative to the other low-index surfaces of copper, one reason being that the surface has the lowest value of surface energy and is therefore most stable among the surfaces of copper metal. There are less studies in the process of Cu(111) oxidation (Ho and Vook 1978, Spitzer and Lüth 1982b, Jensen et al. 1991, 1992, Matsumoto et al. 2001, Wiame et al. 2007).

The observations are quite consistent with each other. Many researchers have observed the copper oxide films to form epitaxially on Cu(111) surface after exposure to oxygen gas and subsequent annealing. The structure of thus formed Cu_2O surface film has been reported to be well-ordered on a short length-scale, with the main structure motives resembling those shown in Figure 3-1(f). The Cu_2O overlayer structure shown in the right-hand side of the figure is an idealization, which does not fully realize because of the too large misfit between the lattice parameters of Cu and Cu_2O. A good matching of the two crystal structures can be achieved by introducing defects that disorder and/or distort that "ideal" structure. As a result, one gets structures that are either disordered on the long-range length scale, or two long-range ordered structures (Jensen et al. 1991, 1992) with large surface unit cells, one of which is $(\sqrt{13}R46.1^\circ \times 7R21.8^\circ)$ so-called '29' superstructure that is 29 times as big as the unit cell of clean Cu(111) shown in Figure 3-1(c), and the other is $(\sqrt{73}R5.8^\circ \times \sqrt{21}R-10.9^\circ)$ so-called '44' superstructure. The two surface reconstructions exhibit distinct honeycomb patterns, identified by Jensen et al. (1992) as distorted honeycomb units of the "ideal" $Cu_2O(111)$ overlayer shown in Figure 3-1(f).

Like in the case of Cu(110) surface, the oxide film growth process on Cu(111) is found to involve surface mobility of copper adatoms that are ejected from step edges and terraces (Matsumoto et al. 2001, Wiame et al. 2007). The process is most rapid in the close packed direction of the surface and leads to mesoscopic changes in surface morphology.

3.2 Oxidation in aqueous solutions

Cuprous oxide becomes thermodynamically stable in aqueous solutions at potentials $E > 0.58-0.059\cdot$pH (Pourbaix 1974). At higher potentials, $E > 0.78-0.059\cdot$pH (for pH>5), a duplex film of $Cu_2O|CuO,Cu(OH)_2$ starts to form. An overview of the adsorbed layer structures formed on low-index metal surfaces in various aqueous solutions can be found in a recent review paper (Magnussen 2002). Spectroscopic analyses of the films formed on copper in aqueous solutions relevant for the repository conditions were performed recently (Kvashnina et al. 2007a, b).

The stability range of adsorbed hydrogen, hydroxyl, and water species on copper exposed to water has been recently studied (Protopopoff and Marcus 2005). A possible role of adsorbed OH species in the process of localized (pitting) corrosion of copper has been discussed by Marcus et al. (2008). Adsorption of water to some copper surfaces has been shown to produce mixed hydroxyl-water layers. An extensive review on this subject can be found in review paper by Hodgson and Haq (2009).

Initial stages of Cu oxidation are usually studied at potentials *negative* to the formation Cu_2O, i.e. in the potential range where a bulk Cu_2O is unstable, but chemisorption of oxygen to the copper surface may occur. Such studies will be briefly reviewed below in this Section. A principal difference exists between copper surface oxidation in oxygen gas and in aqueous solutions, namely, the presence of other species dissolved in water, such as Cl^-, H^+, or OH^-, makes it difficult to identify the chemical composition of the chemisorbed phases on the surface. The Cl^- ion seems to have the strongest effect: it induces a formation of chloride phase (CuCl, cubic zinkblende structure).

3.2.1 Cu(100) surface

Atomic force microscopy (AFM) study on Cu(100) crystals reported a $c(2\times2)$ structure attributed to adsorbed oxygen species at a pH near 1. However, the Cl^- adlattice on this surface also exhibited a $c(2\times2)$ structure making it impossible to definitely distinguish between chlorine and oxygen (Cruickshank et al. 1993). However, Galeotti et al. (1996) found that chlorine chemisorbed to Cu(100) surface forms a cubic zinkblend structure of CuCl with the (111) plane parallel to the substrate surface. The CuCl (111) polar surface is found to be Cl-terminated.

In situ STM study of the anodic oxidation of Cu(100) in 0.1 M aqueous solution of NaOH has reported several surface-reconstructed patterns that involve dimers of Cu atoms ejected from the substrate and stabilized by adsorbed OH groups. The dimers are alternatively aligned along the directions to form zig-zag arrangements. The process of conversion of these adsorbed films into Cu_2O overlayers has been monitored in situ (Kunze et al. 2003).

3.2.2 Cu(110) surface

Adsorption of water to Cu(110) surface is partially dissociative even at room temperature according to Ammon et al. (2003) and Andersson et al. (2005), which leads to the formation of mixed hydroxyl-water adlayers (Yamamoto et al. 2007, Andersson et al. 2007, Hodgson and Haq 2009). Two possible configuration of adsorbed hydroxyl species have been proposed to exist on the basis of infra-red spectroscopic data, H-up and H-down, and their energies were calculated to differ by less than 40 meV (Schiros et al. 2006). More accurate calculations, including corrections for zero-point energy, have been used to refine the value of the dissociation barrier as well as to compute the relative stability of several ordered structures at different degrees of Cu(110) surface coverage (Tang and Chen 2007b). The faith of hydrogen, which must also be produced as a result of dissociative water adsorption, is not quite clear. It may escape from the surface, remain in an adsorbed state, or go sub-surface where it may become locked in (Waugh 2004).

The growth of oxygen adlayers on Cu(110) surface has been observed in pH 2.5−2.7 $HClO_4$ and H_2SO_4 solutions (thermodynamic potential-pH considerations suggest that a bulk oxide is unstable at pH < 3.5 at the open circuit potential). Similar to the case of UHV studies, a growth of …Cu-O-Cu-O… chains in the [001] direction was observed. The chains are found to arrange themselves into (2×1) and (3×1) structures, both in the sulfate and perchlorate electrolyte. The occurrence of the (3×1) reconstruction, which is not seen in UHV experiments, may be due to a Cl^- contaminant that is present in both electrolytes or due to co-adsorbed hydroxide species (LaGraff and Gewirth 1995).

The structure of mixed water-hydroxyl layers on the Cu(110) *c*(2×2) reconstructed surface has been studied using scanning tunneling microscopy and *ab initio* calculations (Forster et al. 2011). The authors found that, instead of forming a complete hydrogen bonding network corresponding to the stoichiometric *c*(2×2) H_2O-OH phase, structures containing an excess of water over hydroxyl are stabilized on Cu(110) by forming a distorted hexagonal network of water-hydroxyl trimers containing D-type Bjerrum defects (two H atoms, instead of one, situated between two adjacent O atoms). This arrangement is argued to maximize the number of strong bonds formed by water donation to OH, thus providing uncoordinated OH groups able to hydrogen bond multilayer water and stabilizing water adsorption at the metal surface (Forster et al. 2011).

3.2.3 Cu(111) surface

Water adsorption to the low-energy Cu(111) surface is not dissociative, and that may be the reason why this surface is hydrophobic. Clusters of water were observed experimentally on the surface (Michaelides and Morgenstern 2007), and their ice-like structures were examined using first-principles calculations (Michaelides and Morgenstern 2007, Tang and Chen 2007a).

The growth of oxygen adlayer on Cu(111) in 0.1 M NaOH has been studied in the underpotential range of Cu_2O formation (Maurice et al. 2000). Adsorption and desorption processes are observed at the reversible potential of −0.675−0.02 V/SHE. These processes are initiated preferentially at the step edges on the upper terrace side. The adsorption decreases the mobility of the Cu atoms along the step edges. It also includes the lateral growth of the terraces, which is a result of accumulation, at the step edges, of Cu atoms ejected from the adlayer superstructure due to reconstruction of the outermost Cu plane of the substrate. The same mechanism leads, in the last stages of the adsorption process, to the formation of islands of Cu adatoms on the terraces. The adlayer forms an ordered superstructure [either the $(\sqrt{21}\times\sqrt{21})R10°$ or $(\sqrt{49}\times\sqrt{49})R20°$ superstructures] with a hexagonal lattice having a unit vector of 6 Å and one adspecies per unit cell (coverage $\Theta \cong 0.2$ ML). The lattice parameters suggest that that the outermost Cu plane is reconstructed according to the Cu plane in $Cu_2O(111)$, i.e. with Cu-Cu distances of ≅ 3 Å, with the adlayer forming a (2×2) lattice. The comparison between the STM data and the charge transfer measurements indicates that the adspecies are hydroxide or hydroxyl groups rather than adsorbed oxygen.

3.3 Surfaces of Cu_2O

The atomic and electronic structure of clean and oxygen-dosed of Cu_2O single crystal surfaces were studied experimentally (Schulz and Cox 1991, Önsten et al. 2009). The non-polar unreconstructed (111) surface is found to be quite stable against ion bombardment and annealing in vacuum. The polar $Cu_2O(100)$ surface could be prepared as Cu-rich or O-rich (depending on the O exposure) and was found to exhibit various reconstruction patterns depending on the oxidation degree and annealing history (Schulz and Cox 1991).

Adsorption of various species, such as CO, H_2O, H_2, and propene on Cu_2O single crystal surfaces was also studied (Cox and Schulz 1991a, b, Schulz and Cox 1992a, b). Remarkable changes of Cu_2O single crystal morphology were reported to occur in aqueous solutions containing copper nitrate, ammonium sulphate, and sodium chloride in different concentrations (Siegfried and Choi 2006).

Quite many *ab initio* studies of low-index surfaces of Cu_2O were performed recently (Soon et al. 2006, 2007a, b, Islam et al. 2009a, b, Altarawneh et al. 2009). These studies typically employed gradient-corrected DFT approximations to model the geometry of clean surfaces (polar as well as non-polar) and surfaces with adsorbed molecules (typically, oxygen or water). The results of the structural modeling seem to be trustworthy, while some findings regarding the electronic structure, like that about "multifarious" magnetism of oxygen in copper-deficient Cu_2O, are most likely due to limitations of the DFT approximations used (because experimentally one finds that in copper oxides copper ions become paramagnetic when their oxidation state changes from 1+ to 2+, but not oxygen ions). Calculations using more advanced exchange-correlation functionals must clarify this situation.

Conclusions

1. The electronic structure and ground-state properties of the stoichiometric, defect-free Cu_2O are reproduced reasonably well by the first-principles methods based on density functional theory, except for the fundamental band gap which is strongly underestimated (0.6 eV *vs*. 2.17 eV). Approaches going beyond standard LDA or GGA schemes (such as SIC, LDA+*U*, *GW*, or hybrid functional approaches) are necessary in order to get the fundamental band gap value correctly. Such approaches are essential for describing the energetics of point defects in copper oxides.
2. Plenty of new experimental information concerning the defect structure in non-stoichiometric Cu_2O is available, but the issue is still controversial. All existing models agree that copper vacancies to be the constitutional defects in copper-deficient nonstoichiometric cuprite ($Cu_{2-\delta}O$). There is no general agreement about other neutral or charged defect species in cuprite.
3. The defect models of cuprite developed by Xue and Dieckmann (1990) and Porat and Riess (1994, 1995) seem to be quite flexible so that they give fair descriptions of the electrical and ionic mobilities of cuprite in a wide range of temperatures and oxygen pressures. First-principles calculations are becoming accurate enough to be able to make semi-quantitative predictions regarding the defect structure (Raebiger et al. 2007, Scanlon and Watson 2011) and ionic mobilities (Wright and Nelson 2002).
4. Recent scientific publications provide information on the structure of adsorbed oxygen, copper, hydroxyl, water, and other species on copper surfaces, as well as the data on their surface mobilities. This kind of data may be useful in the analysis of various mechanisms proposed for stress-corrosion cracking of copper.
5. The results of experimental and theoretical studies of the initial stages of copper oxidation in aqueous solutions have been reviewed. Experimental data are available for low-pH solutions and potentials negative to the Cu_2O stability range. Under such conditions, a co-adsorption of chlorine, hydroxide, and hydroxyl species has been observed.

Acknowledgments

Authors wish to thank Lars Werme and Christina Lilja for useful discussions and constant interest to this work. This work has been funded by Svensk Kärnbränslehantering AB, The Swedish Nuclear Fuel and Waste Management Company.

References

SKB's (Svensk Kärnbränslehantering AB) publications can be found at www.skb.se/publications.

Abrikosov I A, Simak S I, Johansson B, Ruban A V, Skriver H L, 1997. Locally self-consistent Green's function approach to the electronic structure problem. Physical Review B, 56, pp 9319–9334.

Altarawneh M, Radny M, Smith P V, Mackie J C, Kennedy E M, Dlugogorski B Z, Soon A, Stampfl C, 2009. A first-principles density functional study of chlorophenol adsorption on CuO(110):CuO. Journal of Chemical Physics, 130, 184505. doi:10.1063/1.3123534

Ammon C, Bayer A, Steinrük H-P, Held G, 2003. Low-temperature partial dissociation of water on Cu(110). Chemical Physics Letters, 377, pp 163–169.

Andersen O K, 1975. Linear methods in band theory. Physical Review B, 12, pp 3060–3083.

Andersson K, Gómez A, Glover C, Nordlund D, Öström H, Schiros T, Takahashi O, Ogasawara H, Pettersson L G M, Nilsson A, 2005. Molecularly intact and dissociative adsorption of water on clean Cu(110): A comparison with the water/Ru(001) system. Surface Science, 585, pp L183–L189.

Andersson K, Ketteler G, Bluhm H, Yamamoto S, Ogasawara H, Pettersson L G M, Salmeron M, Nilsson A, 2007. Bridging the pressure gap in water and hydroxyl chemistry on metal surfaces: the Cu(110) case. Journal of Physical Chemistry C, 111, pp 14493–14499.

Barman S R, Sarma D D, 1992. Investigation of the L_3–$M_{45}M_{45}$ Auger spectra of Cu, Cu_2O, and CuO. Journal of Physics: Condensed Matter, 4, pp 7607–7616.

Baroni S, de Gironcoli S, Corso A D, Gianozzi P, 2001. Phonons and related crystal properties from density-functional perturbation theory. Reviews of Modern Physics, 73, pp 515–562.

Baroni S, Giannozzi P, Isaev E, 2010. Density-functional perturbation theory for quasi-harmonic calculations. Reviews in Mineralogy and Geochemistry, 71, pp 39–57.

Baumeister P W, 1961. Optical absorption of cuprous oxide. Physical Review, 121, pp 359–362.

Beg M M, Shapiro S M, 1976. Study of phonon dispersion relations in cuprous oxide by inelastic neutron scattering. Physical Review B, 13, pp 1728–1734.

Berge K, Goldmann A, 2003. Electronic interchain interactions of the Cu(110)(2×1)O surface – an angle-resolved photoemission study. Surface Science, 540, pp 97–106.

Besenbacher F, Nørskov J K, 1993. Oxygen chemisorption on metal surfaces: General trends for Cu, Ni and Ag. Progress in Surface Science, 44, pp 5–66.

Bessekhouad Y, Robert D, Weber J-V, 2005. Photocatalytic activity of Cu_2O/TiO_2, Bi_2O_3/TiO_2 and $ZnMn_2O_4/TiO_2$ heterojunctions. Catalysis Today, 101, pp 315–321.

Blanchard N P, Martin D S, Weightman P, 2005. Molecular adsorbate induced restructuring of a stepped Cu(110) surface. Physical Status Solid C, 12, pp 4017–4021.

Bloem J, 1958. Discussion of some optical and electrical properties of Cu_2O. Philips Research Reports, 13, pp 167–193.

Blöchl P E, Jepsen O, Andersen O K, 1994. Improved tetrahedron method for Brillouin-zone integrations. Physical Review B, 49, pp 16223–16233.

Bobrov K, Guillemot L, 2008. Interplay between adsorbate-induced reconstruction and local strain: Formation of phases on the Cu(110)-(2×1):O surface. Physical Review B, 78, 121408(R). doi:10.1103/PhysRevB.78.121408

Bohnen K-P, Heid R, Pintschovius L, Soon A, Stampfl C, 2009. *Ab initio* lattice dynamics and thermal expansion of Cu_2O. Physical Review B, 80, 134304. doi:10.1103/PhysRevB.80.134304

Boucher R, 2005a. The electrical property dependence of disordered copper oxide on oxygen content. Journal of Physics and Chemistry Solids, 66, pp 1234–1239.

Boucher R, 2005b. The structural and optical property dependence of disordered copper oxide on oxygen content. Journal of Physics and Chemistry Solids, 66, pp 906–910.

Brandstetter T, Draxler M, Hohage M, Zeppenfeld P, 2008. Oxygen-induced restructuring of Cu(19 19 1) studied by scanning tunneling microscopy. Physical Review B, 78, 075402. doi:10.1103/PhysRevB.78.075402

Brattain W H, 1951. The copper oxide rectifier. Reviews of Modern Physics, 23, pp 203–212.

Breeman M, Boerma D O, 1992. Migration of Cu adatoms on a Cu(100) surface, studied with low-energy ion scattering (LEIS). Surface Science, 269-270, pp 224–228.

Brown K E R, Choi K-S, 2006. Electrochemical synthesis and characterization of transparent nanocrystalline Cu_2O films and their conversion to CuO films. Chemical Communications, 31, pp 3311–3313.

Bruneval F, Vast N, Reining L, Izquierdo M, Sirotti F, Barrett N, 2006. Exchange and correlation effects in electronic excitations of Cu_2O. Physical Review Letters, 97, 267601. doi:10.1103/PhysRevLett.97.267601

Buljan A, Llunell M, Ruiz E, Alemany P, 2001. Color and conductivity in Cu_2O and $CuAlO_2$: a theoretical analysis of $d^{10}...d^{10}$ interactions in solid-state compounds. Chemistry of Materials, 13, pp 338–344.

Burlakov V M, Göppert M, Jolk A, Dinger A, Becker R, Klingshirn C F, 1999. On a biophotonic origin of the 1125 cm^{-1} absorption band in cuprous oxide. Physics Letters A, 254, pp 95–100.

Chaika A N, Nazin S S, Bozhko S I, 2008. Selective STM imaging of oxygen-induced Cu(115) surface reconstructions with tungsten probes. Surface Science, 602, pp 2078–2088.

Chase M W, 1998. NIST-JANAF thermochemical tables. Part II, Cr–Zr. 4th ed. New York: American Institute of Physics.

Ching W Y, Xu Y-N, Wong K W, 1989. Ground-state and optical properties of Cu_2O and CuO crystals. Physical Review B, 40, pp 7684–7595.

Coulman D J, Wintterlin J, Behm R J, Ertl G, 1990. Novel mechanism for the formation of chemisorption phases: The (2×1)O-Cu(110) "added row" reconstruction. Physical Review Letters, 64, pp 1761–1764.

Cox D, Schulz K H, 1991a. H_2O adsorption on $Cu_2O(100)$. Surface Science, 256, pp 67–76.

Cox D F, Schulz K H, 1991b. Interaction of CO with Cu^+ cations: CO adsorption on $Cu_2O(100)$. Surface Science, 249, pp 138–148.

Cruickshank B, Sneddon D D, Gewirth A A, 1993. In situ observations of oxygen adsorption on a Cu(100) substrate using atomic force microscopy. Surface Science Letters, 281, pp 308–314.

Dapiaggi M, Tiano W, Artioli G, Sanson A, Fornasini P, 2003. The thermal behaviour of cuprite: An XRD–EXAFS combined approach. Nuclear Instruments and Methods in Physics Research Section B, 200, pp 231–236.

Dash L K, Bruneval F, Trinité V, Vast N, Reining L, 2007. Electronic excitations: ab initio calculations of electronic spectra and application to zirconia ZrO_2, titania TiO_2 and cuprous oxide Cu_2O. Computational Materials Science, 38, pp 482–493.

Dawson P, Hargreave M M, Wilkinson G R, 1973. The dielectric and lattice vibrational spectrum of cuprous oxide. Journal of Physics and Chemistry of Solids, 34, pp 2201–2208.

de Jongh P E, Vanmaekelbergh D, Kelly J J, 1999. Cu_2O: a catalyst for the photochemical decomposition of water? Chemical Communications, 1999, pp 1069–1070.

De Miguel J J, Sánchez A, Cebollada A, Gallego J M, Ferrón J, Ferrer S, 1987. The surface morphology of a growing crystal studied by thermal energy atom scattering (TEAS). Surface Science, 189–190, pp 1062–1068.

Dieckmann R, 1998. Point defects and transport in non-stoichiometric oxides: solved and unsolved problems. Journal of Physics and Chemistry of Solids, 59, pp 507–525.

Dünwald H, Wagner C, 1933. Influence of constitution of cuprous oxide on electrical properties. Zeitschrift für Physikalische Chemie, 22, pp 212–215.

Dürr H, Wendelken J F, Zuo J-K, 1995. Island morphology and adatom energy barriers during homoepitaxy on Cu(001). Surface Science, 328, pp L527–L532.

Elliott R J, 1957. Intensity of optical absorption by excitons. Physical Review, 108, pp 1384–1389.

Elliott R J, 1961. Symmetry of excitons in Cu_2O. Physical Review, 124, pp 340–345.

Ertl G, 1967. Untersuchung von oberflächenreaktionen mittels beugung langsamer elektronen (LEED): I. Wechselwirkung von O_2 und N_2o mit (110)-, (111)- und (100)-Kupfer-Oberflächen. Surface Science, 6, pp 208–232.

Feng Y, Teo W-K, Siow K-S, Tan K-L, Hsieh A-K, 1996a. The corrosion behaviour of copper in neutral tap water. Part I: Corrosion mechanisms. Corrosion Science 38, pp 369–385.

Feng Y, Teo W-K, Siow K-S, Hsieh A-K, 1996b. The corrosion behaviour of copper in neutral tap water. Part II: Determination of corrosion rates. Corrosion Science 38, pp 387–395.

Filippetti A, Fiorentini V, 2005a. Coexistence of ionic and metallic bonding in noble-metal oxides. Physical Review B, 72, 035128. doi:10.1103/PhysRevB.72.035128

Filippetti A, Fiorentini V, 2005b. Magnetic ordering in CuO from first principles: A cuprate antiferromagnet with fully three-dimensional exchange interactions. Physical Review Letters, 95, 086405. doi:10.1103/PhysRevLett.95.086405

Fornasini P, Dalba G, Grisenti R, Purans J, Vaccari M, Rocca F, Sanson A, 2006. Local behaviour of negative thermal expansion materials. Nuclear Instruments and Methods in Physics Research Section B, 246, pp 180–183.

Forster M, Raval R, Hodgson A, Carrasco J, Michaelides A, 2011. *c*(2×2) water-hydroxyl layer on Cu(110): a wetting layer stabilized by Bjerrum defects. Physical Review Letters, 106, 046103. doi:10.1103/PhysRevLett.106.046103

Fujita T, Okawa Y, Matsumoto Y, Tanaka K, 1996. Phase boundaries of nanometer scale *c*(2×2)-O domains on the Cu(100) surface. Physical Review B, 54, pp 2167–2174.

Galeotti M, Cortigiani B, Torrini M, Bardi U, Andryushechkin B, Klimov A, Eltsov K, 1996. Epitaxy and structure of the chloride phase formed by reaction of chlorine with Cu(100): a study by X-ray photoelectron diffraction. Surface Science, 349, pp L164–L168.

Ghijsen J, Tjeng L H, van Elp J, Eskes H, Westerink J, Sawatzky G A, Czyzyk M, 1988. Electronic structure of Cu_2O and CuO. Physical Review B, 38, pp 11322–11330.

Giannozzi P, Baroni S, Bonini N, Calandra M, Car R, Cavazzoni C, Ceresoli D, Chiarotti G L, Cococcioni M, Dabo I, Dal Corso A, de Gironcoli S, Fabris S, Fratesi G, Gebauer R, Gerstmann U, Gougoussis C, Kokalj A, Lazzeri M, Martin-Samos L, Marzari N, Mauri F, Mazzarello R, Paolini S, Pasquarello A, Paulatto L, Sbraccia C, Scandolo S, Sclauzero G, Seitsonen A P, Smogunov A, Umari P, Wentzcovitch R M, 2009. QUANTUM ESPRESSO: a modular and open-source software project for quantum simulations of materials. Journal of Physics: Condensed Matter, 21, 395502. doi:10.1088/0953-8984/21/39/395502

Gregor L V, 1962. The heat capacity of cuprous oxide from 2.8 to 21°K. Journal of Physical Chemistry, 66, pp 1645–1647.

Hallberg J, Hanson R C, 1970. The elastic constants of cuprous oxide. Physica Status Solidi B, 42, pp 305–310.

Hara M, Kondo T, Komoda M, Ikeda S, Shinohara K, Tanaka A, Kondo J N, Domen K, 1998. Cu_2O as a photocatalyst for overall water splitting under visible light irradiation. Chemical Communications, 1998, pp 357–358.

Harrison M J, Woodruff D P, Robinson J, Sander D, Pan W, Kirschner J, 2006. Adsorbate-induced surface reconstruction and surface-stress changes in Cu(100)/O: Experiment and theory. Physical Review B, 74, 165402. doi:10.1103/PhysRevB.74.165402

Haugsrud R, 2002. The influence of water vapor on the oxidation of copper at intermediate temperatures. Journal of the Electrochemical Society, 149, pp B14–B21.

Haugsrud R, Kofstad P, 1997. On the oxygen pressure dependence of high temperature oxidation of copper. Materials Science Forum 251–254, pp 65–72.

Haugsrud R, Norby T, 1999. Determination of thermodynamics and kinetics of point defects in Cu_2O using the Rosenburg method. Journal of the Electrochemical Society, 146, pp 999–1004.

Ho J H, Vook R W, 1978. (111)Cu_2O growth modes on (111)Cu surfaces. Journal of Crystal Growth, 44, pp 561–569.

Hodgson A, Haq S, 2009. Water adsorption and the wetting of metal surfaces. Surface Science Reports, 64, pp 381–451.

Hohenberg P, Kohn W, 1964. Inhomogeneous electron gas. Physical Review, 136, pp B864–B871.

Hu C-C, Nian J-N, Teng H, 2008a. Electrodeposited p-type Cu_2O as photocatalyst for H_2 evolution from water in the presence of WO_3. Solar Energy Materials and Solar Cells, 92, pp 1071–1076.

Hu J-H, Johnston H L, 1951. Low temperature heat capacities of inorganic solids. IX. Heat capacity and thermodynamic properties of cuprous oxide from 14 to 300°K. Journal of the American Chemical Society, 73, pp 4550–4551.

Hu J P, Payne D J, Egdell R G, Glans P-A, Learmonth T, Smith K E, Guo J, Harrison N M, 2008b. On-site interband excitations in resonant inelastic X-ray scattering from Cu_2O. Physical Review B, 77, 155115. doi:10.1103/PhysRevB.77.155115

Hugosson H W, Korzhavyi P A, Jansson U, Johansson B, Eriksson O, 2001. Phase stabilities and structural relaxations in substoichiometric TiC_{1-x}. Physical Review B, 63, 165116. doi:10.1103/PhysRevB.63.165116

Humphreys C J, 1999. Electrons seen in orbit. Nature, 401, pp 21–22.

Ikeda S, Takata T, Kondo T, Hitoki G, Hara M, Kondo J N, Domen K, Hosono H, Kawazoe H, Tanaka A, 1998. Mechano-catalytic overall water splitting. Chemical Communications, 1998, pp 2185–2186.

Islam M M, Diawara B, Maurice V, Marcus P, 2009a. Bulk and surface properties of Cu_2O: A first-principles investigation. Journal of Molecular Structure: THEOCHEM, 903, pp 41–48.

Islam M M, Diawara B, Maurice V, Marcus P, 2009b. First principles investigation on the stabilization mechanisms of the polar copper terminated Cu_2O(111) surface. Surface Science, 603, pp 2087–2095.

Ito T, Yamaguchi H, Okabe K, Masumi T, 1998. Single-crystal growth and characterization of Cu_2O and CuO. Journal of Materials Science, 33, pp 3555–3566.

Ivanda M, Waasmaier D, Endriss A, Ihringer J, Kirfel A, Kiefer W, 1997. Low-temperature anomalies of cuprite observed by raman spectroscopy and x-ray powder diffraction. Journal of Raman Spectroscopy, 28, pp 487–493.

Jacobsen K W, Nørskov J K, 1990. Theory of the oxygen-induced restructuring of Cu(110) and Cu(100) surfaces. Physical Review Letters, 65, pp 1788–1791.

Jensen F, Besenbacher F, Lægsgaard E, Stensgaard I, 1990. Dynamics of oxygen-induced reconstruction of Cu(100) studied by scanning tunneling microscopy. Physical Review B, 42, pp 9206–9209.

Jensen F, Besenbacher F, Læsgaard E, Stensgaard I, 1991. Oxidation of Cu(111): two new oxygen induced reconstructions. Surface Science, 259, pp L774–L780.

Jensen F, Besenbacher F, Stensgaard I, 1992. Two new oxygen induced reconstructions on Cu(111). Surface Science, 269–270, pp 400–404.

Jolk A, Klingshirn C F, 1998. Linear and nonlinear excitonic absorption and photoluminescence spectra in Cu_2O: Line shape analysis and exciton drift. Physica Status Solidi B, 206, pp 841–850.

Kakuta S, Abe T, 2009. Structural characterization of Cu_2O after the evolution of H_2 under visible light irradiation. Electrochemical and Solid-State Letters, 12, pp P1–P3.

Katayama T, Sekiba D, Mukai K, Yamashita Y, Komori F, Yoshinobu J, 2007. Adsorption states and dissociation processes of oxygen molecules on Cu(100) at low temperature. Journal of Physical Chemistry C, 111, pp 15059–15063.

Kirfel A, Eichhorn K, 1990. Accurate structure analysis with synchrotron radiation. The electron density in Al_2O_3 and Cu_2O. Acta Crystallographica Section A, 46, pp 271–284.

Kishimoto S, Kageshima M, Naitoh Y, Li Y J, Sugawara Y, 2008. Study of oxidized Cu(110) surface using noncontact atomic force microscopy. Surface Science, 602, pp 2175–2182.

Kittel C, 1986. Introduction to solid state physics. 6th ed. New York: Wiley.

Kittel M, Polcik M, Terborg R, Hoeft J T, Baumgartel P, Bradshaw A M, Toomes R L, Kang J H, Woodruff D P, Pascal M, Lamont C L A, Rotenberg E, 2001. The structure of oxygen on Cu(100) at low and high coverages. Surface Science, 470, pp 311–324.

Kleinman L, Mednick K, 1980. Self-consistent energy bands of Cu_2O. Physical Review B, 21, pp 1549–1553.

Kohn W, Sham L J, 1965. Self-consistent equations including exchange and correlation effects. Physical Review, 140, pp A1133–A1138.

Korzhavyi P, Johansson B, 2010. Thermodynamic properties of copper compounds with oxygen and hydrogen from first principles. SKB TR-10-30, Svensk Kärnbränslehantering AB.

Korzhavyi P A, Abrikosov I A, Johansson B, Ruban A V, Skriver H L, 1999. First-principles calculations of the vacancy formation energy in transition and noble metals. Physical Review B, 59, pp 11693–11703.

Korzhavyi P A, Ruban A V, Lozovoi A Y, Vekilov Y K, Abrikosov I A, Johansson B, 2000. Constitutional and thermal point defects in B2 NiAl. Physical Review B, 61, pp 6003–6018.

Korzhavyi P A, Pourovskii L V, Hugosson H W, Ruban A V, Johansson B, 2002a. Ab initio study of phase equilibria in TiC_x. Physical Review Letters, 88, 015505. doi:10.1103/PhysRevLett.88.015505

Korzhavyi P A, Abrikosov I A, Smirnova E A, Bergqvist L, Mohn P, Mathieu R, Svedlindh P, Sadowski J, Isaev E I, Vekilov Y K, Eriksson O, 2002b. Defect-induced magnetic structure in $(Ga_{1-x}Mn_x)As$. Physical Review Letters, 88, 187202. doi:10.1103/PhysRevLett.88.187202

Korzhavyi P, Soroka I, Boman M, Johansson B, 2011. Thermodynamics of stable and metastable Cu-O-H compounds. Solid State Phenomena, 172–174, pp 973–978.

Kröger F A, 1964. The chemistry of imperfect crystals. Amsterdam: North-Holland.

Kunze J, Maurice V, Klein L H, Strehblow H-H, Marcus P, 2003. In situ STM study of the anodic oxidation of Cu(001) in 0.1 M NaOH. Journal of Electroanalytical Chemistry, 554–555, pp 113–125.

Kvashnina K O, Butorin S M, Modin A, Soroka I, Marcellini M, Guo J-H, Werme L, Nordgren J, 2007a. Changes in electronic structure of copper films in aqueous solutions. Journal of Physics: Condensed Matter, 19, 226002. doi:10.1088/0953-8984/19/22/226002

Kvashnina K O, Butorin S M, Modin A, Soroka I, Marcellini M, Nordgren J, Guo J-H, Werme L, 2007b. In situ X-ray absorption study of copper films in ground water solutions. Chemical Physics Letters, 447, pp 54–57.

LaGraff J R, Gewirth A A, 1995. In-situ observation of oxygen adlayer formation on Cu(110) electrode surfaces. Surface Science, 326, pp L461–L466.

Lahtonen K, Hirsimäki M, Lampimäki M, Valden M, 2008. Oxygen adsorption-induced nano-structures and island formation on Cu{100}: bridging the gap between the formation of surface confined oxygen chemisorption layer and oxide formation. Journal of Chemical Physics, 129, 124703. doi:10.1063/1.2980347

Laskowski R, Blaha P, Schwarz K, 2003. Charge distribution and chemical bonding in Cu_2O. Physical Review B, 67, 075102. doi:10.1103/PhysRevB.67.075102

Lee R N, Farnsworth H E, 1965. LEED studies of adsorption on clean (100) copper surfaces. Surface Science, 3, pp 461–479.

Liem S Y, Kresse G, Clarke J H R, 1998. First principles calculation of oxygen adsorption and reconstruction of Cu(110) surface. Surface Science, 415, pp 194–211.

Liem S Y, Clarke J H R, Kresse G, 2000. Pathways to dissociation of O_2 on Cu (110) surface: first principles simulations. Surface Science, 459, pp 104–114.

Lippmann T, Schneider J R, 2000a. Accurate structure-factor measurements using high-energy synchrotron radiation: a test on cuprite, Cu_2O. Journal of Applied Crystallography, 33, pp 156–167.

Lippmann T, Schneider J R, 2000b. Topological analyses of cuprite, Cu_2O, using high-energy synchrotron-radiation data. Acta Crystallographica Section A, 56, pp 575–584.

Madsen G K H, Blaha P, Schwarz K, Sjöstedt E, Nordström L, 2001. Efficient linearization of the augmented plane-wave method. Physical Review B, 64, 195134. doi:10.1103/PhysRevB.64.195134

Magnussen O M, 2002. Ordered anion adlayers on metal electrode surfaces. Chemical Reviews, 102, pp 679–725.

Maluenda J, Farhi R, Petot-Ervas G, 1981a. Chemical diffusion measurements in single crystalline cuprous oxide. Journal of Physics and Chemistry of Solids, 42, pp 697–699.

Maluenda J, Farhi R, Petot-Ervas G, 1981b. Electrical conductivity at high temperature and thermodynamic study of point defects in single crystalline cuprous oxide. Journal of Physics and Chemistry of Solids, 42, pp 911–921.

Manghnani M H, Brower W S, Parker H S, 1974. Anomalous elastic behavior in Cu_2O under pressure. Physica Status Solidi A, 25, pp 69–76.

Marcus P, Maurice V, Strehblow H-H, 2008. Localized corrosion (pitting): a model of passivity breakdown including the role of the oxide layer nanostructure. Corrosion Science, 50, pp 2698–2704.

Marksteiner P, Blaha P, Schwarz K, 1986. Electronic structure and binding mechanism of Cu_2O. Zeitschrift für Physik B: Condensed Matter, 64, pp 119–127.

Martínez-Ruiz A, Moreno M G, Takeuchi N, 2003. First principles calculations of the electronic properties of bulk Cu_2O, clean and doped with Ag, Ni, and Zn. Solid State Sciences, 5, pp 291–295.

Matsumoto T, Bennett R A, Stone P, Yamada T, Domen K, Bowker M, 2001. Scanning tunneling microscopy studies of oxygen adsorption on Cu(111). Surface Science, 471, pp 225–245.

Maurice V, Strehblow H-H, Marcus P, 2000. In situ STM study of the initial stages of oxidation of Cu(111) in aqueous solution. Surface Science, 458, pp 185–194.

McDonnell L, Woodruff D P, 1974. A LEED study of oxygen adsorption on copper (100) and (111) surfaces. Surface Science, 46, pp 505–536.

McKinzie H L, O'Keeffe M, 1967. High temperature Hall effect in cuprous oxide. Physical Letters A, 24, pp 137–139.

Michaelides A, Morgenstern K, 2007. Ice nanoclusters at hydrophobic metal surfaces. Nature Materials, 6, pp 597–601.

Mittal R, Chaplot S L, Mishra S K, Bose P P, 2007. Inelastic neutron scattering and lattice dynamical calculation of negative thermal expansion compounds Cu_2O and Ag_2O. Physical Review B, 75, 174303. doi:10.1103/PhysRevB.75.174303

Mocuta D, Ahner J, Lee J-G, Denev S, Yates J T, 1999. Self-organized nanostructures: an ESDIAD study of the striped oxidized Cu(110) surface. Surface Science, 436, pp 72–82.

Moore W J, Selikson B, 1951. The diffusion of copper in cuprous oxide. Journal of Chemical Physics, 19, pp 1539–1543.

Moore W J, Selikson B, 1952. Erratum: The diffusion of copper in cuprous oxide. Journal of Chemical Physics, 20, p 927.

Moss B K, Goodman P, Johnson A W S, 1988. Investigation of mineralogical and synthetic Cu_2O by HREM and CBED. Journal of Solid State Chemistry, 73, pp 268–273.

Musa A O, Akomolafe T, Carter M J, 1998. Production of cuprous oxide, a solar cell material, by thermal oxidation and a study of its physical and electrical properties. Solar Energy Materials and Solar Cells, 51, pp 305–316.

Müser H, Schilling H, 1952. Measurements of thermoelectric power of Cu_2O at high temperatures. Zeitschrift für Naturforschung A, 7, pp 211–212.

Nolan M, Elliott S D, 2006. The p-type conduction mechanism in Cu_2O: a first principles study. Physical Chemistry Chemical Physics, 8, pp 5350–5358.

Ochin P, Petot-Ervas G, Petot C, 1985. Mass transport in cuprous oxide. Journal of Physics and Chemistry of Solids, 46, pp 695–700.

Ochin P, Petot, Perot-Ervas G, 1984. Thermodynamic study of point defects in $Cu_{2-\delta}O$. Electrical conductivity measurements at low oxygen partial pressures. Solid State Ionics, 12, pp 135–143.

O'Keeffe M, 1963. Infrared optical properties of cuprous oxide. Journal of Chemical Physics, 39, pp 1789–1793.

O'Keeffe M, Moore W J, 1961. Electrical conductivity of monocrystalline cuprous oxide. Journal of Chemical Physics, 35, pp 1324–1328.

O'Keeffe M, Moore W J, 1962. Thermodynamics of formation and migration of defects in cuprous oxide. Journal of Chemical Physics, 36, pp 3009–3013.

Olsen L C, Addis F W, Miller W, 1982. Experimental and theoretical studies of Cu_2O solar cells. Solar Cells, 7, pp 247–279.

Orgel L E, 1958. 843. Stereochemistry of metals of the B sub-groups. Part I. Ions with filled d-electron shells. Journal of Chemical Society, 1958, pp 4186–4190.

Oustry A, Lafourcade L, Escaut A, 1973. Étude par del de l'interaction de l'oxygène avec les faces (110), (100) et (111) de monocristaux de cuivre. Surface Science, 40, pp 545–554.

Park J-H, Natesan K, 1993. Oxidation of copper and electronic transport in copper oxides. Oxidation of Metals, 39, pp 411–435.

Perdew J P, Burke K, Ernzerhof M, 1996. Generalized gradient approximation made simple. Physical Review Letters, 77, pp 3865–3868.

Peterson N L, Wiley C L, 1984a. Diffusion and point defects in Cu_2O. Journal of Physics and Chemistry of Solids, 45, pp 281–294.

Peterson N L, Wiley C L, 1984b. Silver-tracer diffusion in Cu_2O. Journal of Physics and Chemistry of Solids, 45, pp 295–298.

Piippo J, Saario T, Laitinen T, Bojinov M, Hinttala J, 1998. Electrical properties of surface films formed on copper. Material Science Forum, 289–292, pp 429–438.

Porat O, Riess I, 1994. Defect chemistry of $Cu_{2-y}O$ at elevated temperatures. Part I: Non-stoichiometry, phase width and dominant point defects. Solid State Ionics, 74, pp 229–238.

Porat O, Riess I, 1995. Defect chemistry of $Cu_{2-y}O$ at elevated temperatures. Part II: Electrical conductivity, thermoelectric power and charged point defects. Solid State Ionics, 81, pp 29–41.

Pourbaix M, 1974. Atlas of electrochemical equilibria in aqueous solutions. 2nd ed. Houston, TX: National Association of Corrosion Engineers.

Prévot G, Croset B, Girard Y, Coati A, Garreau Y, Sun L D, Hohage M, Zeppenfeld P, 2004. Elastic origin of the O/Cu(110) self-ordering evidenced by GIXD. Surface Science, 549, pp 52–66.

Protopopoff E, Marcus P, 2005. Potential–pH diagrams for hydroxyl and hydrogen adsorbed on a copper surface. Electrochimica Acta, 51, pp 408–417.

Raebiger H, Lany S, Zunger A, 2007. Origins of the p-type nature and cation deficiency in Cu_2O and related materials. Physical Review B, 76, 045209. doi:10.1103/PhysRevB.76.045209

Rai B P, 1988. Cu_2O solar cells: a review. Solar Cells, 25, pp 265–272.

Rakhshani A E, 1986. Preparation, characteristics and photovoltaic properties of cuprous oxide – a review. Solid-State Electronics, 29, pp 7–17.

Reinecke N, Taglauer E, 2000. The kinetics of oxygen-induced faceting of Cu(115) and Cu(119) surfaces. Surface Science, 454–456, pp 94–100.

Robertson J, 1983. Electronic structure and x-ray near-edge core spectra of Cu_2O. Physical Review B, 28, pp 3378–3385.

Rosenstock Z, Riess I, 2000. Preparation of oxide thin films by controlled diffusion of oxygen atoms. Solid State Ionics, 136–137, pp 921–926.

Rous P J, 1995. Surface crystallography: the experimental data base. In: Binder K, Bowker M, Inglesfield J E, Rous P J (eds). Cohesion and structure of surfaces. Amsterdam: Elsevier Science. (Cohesion and Structure 4), pp 1–61.

Ruban A V, Skriver H L, 1999. Calculated surface segregation in transition metal alloys. Computational Materials Science, 15, pp 119–143.

Ruiz E, Alvarez S, Alemany P, Evarestov R, 1997. Electronic structure and properties of Cu_2O. Physical Review B, 56, 7189–7196.

Savrasov S Y, 1996. Linear-response theory and lattice dynamics: A muffin-tin-orbital approach. Physical Review B, 54, pp 16470–16486.

Savrasov S Y, Savrasov D Y, 1996. Full-potential linear-muffin-tin-orbital method for calculating total energies and forces. Physical Review B, 46, pp 12181–12195.

Scanlon D O, Watson G W, 2011. Uncovering the complex behavior of hydrogen in Cu_2O. Physical Review Letters, 106, 186403. doi:10.1103/PhysRevLett.106.186403

Schick J D, Trivich D, 1971. Photokinetics in single-crystal cuprous oxide. Chemical Physics Letters, 10, pp 465–467.

Schiros T, Haq S, Ogasawara H, Takahashi O, Ostrom H, Andersson K, Pettersson L, Hodgson A, Nilsson A, 2006. Structure of water adsorbed on the open Cu(110) surface: H-up, H-down, or both? Chemical Physics Letters, 429, pp 415–419.

Schulz K H, Cox D F, 1991. Photoemission and low-energy-electron-diffraction study of clean and oxygen-dosed Cu_2O (111) and (100) surfaces. Physical Review B, 43, pp 1610–1621.

Schulz K H, Cox D F, 1992a. Propene adsorption on Cu_2O single-crystal surfaces. Surface Science, 262, pp 318–334.

Schulz K H, Cox D F, 1992b. Surface hydride formation on a metal oxide surface: the interaction of atomic hydrogen with $Cu_2O(100)$. Surface Science, 278, pp 9–18.

Schäfer W, Kirfel A, 2002. Neutron powder diffraction study of the thermal expansion of cuprite. Applied Physics A Materials Science & Processing, 74, Suppl 1, pp S1010–S1012.

Serin N, Serin T, Horzum Ş, Çelik Y, 2005. Annealing effects on the properties of copper oxide thin films prepared by chemical deposition. Semiconductor Science and Technology, 20, pp 398–401.

Shannon R D, 1976. Revised effective ionic radii and systematic studies of interatomic distances in halides and chalcogenides. Acta Crystallographica Section A, 32, pp 751–767.

Shen Z-X, List R S, Dessau D S, Parmigiani F, Arko A J, Bartlett R, Wells B O, Lindau I, Spicer W E, 1990. Photoemission study of CuO and Cu_2O single crystals. Physical Review B, 42, pp 8081–8085.

Shockley W, Last J T, 1957. Statistics of the charge distribution for a localized flaw in a semiconductor. Physical Review, 107, pp 392–396.

Sieberer M, Redinger J, Mohn P, 2007. Electronic and magnetic structure of cuprous oxide Cu_2O doped with Mn, Fe, Co, and Ni: A density-functional theory study. Physical Review B, 75, 035203. doi:10.1103/PhysRevB.75.035203

Siegfried M J, Choi K-S, 2006. Elucidating the effect of additives on the growth and stability of Cu_2O surfaces via shape transformation of pre-grown crystals. Journal of the American Chemical Society, 128, pp 10356–10357.

Simmons G W, Mitchell D F, Lawless K R, 1967. LEED and HEED studies of the interaction of oxygen with single crystal surfaces of copper. Surface Science, 8, pp 130–164.

Siripala W, Ivanovskaya A, Jaramillo T F, Baeck S-H, McFarland E W, 2003. A Cu_2O/TiO_2 heterojunction thin film cathode for photoelectrocatalysis. Solar Energy Materials and Solar Cells, 77, pp 229–237.

Smyth J R, Jacobsen S D, Hazen R M, 2000. Comparative crystal chemistry of dense oxide minerals. In: Hazen R M, Downs R T (eds). High-temperature and high-pressure crystal chemistry. Washington, DC: Mineralogical Society of America. (Reviews in Mineralogy & Geochemistry 41), pp 157–186.

Somasundaram S, Chenthamarakshan C R N, de Tacconi N R, Rajeshwar K, 2007. Photocatalytic production of hydrogen from electrodeposited p-Cu_2O film and sacrificial electron donors. International Journal of Hydrogen Energy, 32, pp 4661–4669.

Soon A, Todorova M, Delley B, Stampfl C, 2006. Oxygen adsorption and stability of surface oxides on Cu(111): a first-principles investigation. Physical Review B, 73, 165424. doi:10.1103/PhysRevB.73.165424

Soon A, Todorova M, Delley B, Stampfl C, 2007a. Thermodynamic stability and structure of copper oxide surfaces: a first-principles investigation. Physical Review B, 75, 125420. doi:10.1103/PhysRevB.75.125420

Soon A, Todorova M, Delley B, Stampfl C, 2007b. Erratum: Thermodynamic stability and structure of copper oxide surfaces: a first-principles investigation. Physical Review B, 76, 129902(E). doi:10.1103/PhysRevB.76.129902

Soon A, Cui X-Y, Delley B, Wei S-H, Stampfl C, 2009. Native defect-induced multifarious magnetism in nonstoichiometric cuprous oxide: first-principles study of bulk and surface properties of $Cu_{2-\delta}O$. Physical Review B, 79, 035205. doi:10.1103/PhysRevB.79.035205

Spitzer A, Lüth H, 1982a. The adsorption of oxygen on copper surfaces: I. Cu(100) and Cu(110). Surface Science, 118, pp 121–135.

Spitzer A, Lüth H, 1982b. The adsorption of oxygen on copper surfaces: II. Cu(111). Surface Science, 118, pp 136–144.

Sun L D, Hohage M, Denk R, Zeppenfeld P, 2007. Oxygen adsorption on Cu(110) at low temperature. Physical Review B, 76, 245412. doi:10.1103/PhysRevB.76.245412

Tanaka K, Fujita T, Okawa Y, 1998. Oxygen induced order–disorder restructuring of a Cu(100) surface. Surface Science, 401, pp L407–L412.

Tang Q-L, Chen Z-X, 2007a. Density functional slab model studies of water adsorption on flat and stepped Cu surfaces. Surface Science, 601, pp 954–964.

Tang Q-L, Chen Z-X, 2007b. Influence of aggregation, defects, and contaminant oxygen on water dissociation at Cu(110) surface: a theoretical study. Journal of Chemical Physics, 127, 104707. doi:10.1063/1.2751154

Taylor J C W, Weichman F L, 1969. Role of excitons in the luminescence of cuprous oxide. Physical Review, 185, pp 1214–1217.

Tiano W, Dapiaggi M, Artioli G, 2003. Thermal expansion in cuprite-type structures from 10 K to decomposition temperature: Cu_2O and Ag_2O. Journal of Applied Crystallography, 36, pp 1461–1463.

Timm H, Janek J, 2005. On the Soret effect in binary nonstoichiometric oxides – kinetic demixing of cuprite in a temperature gradient. Solid State Ionics, 176, pp 1131–1143.

Tomlinson W J, Yates J, 1977. The diffusion of Cu in copper(I) oxide. Journal of Physics and Chemistry of Solids, 38, pp 1205–1206.

Toth R S, Kilkson R, Trivich D, 1961. Electrical conductivity of single-crystal cuprous oxide at high temperatures. Physical Review, 122, pp 482–488.

Tretyakov Y D, Komarov V F, Prosvirina N A, Kutsenok I B, 1972. Nonstoichiometry and defect structures in copper oxides and ferrites. Journal of Solid State Chemistry, 5, pp 157–167.

Tsur Y, Riess I, 1998. Impurity solubility limits in ionic crystals, with application to Cu_2O. Zeitschrift für Physikalische Chemie, 207, pp 181–213.

Tsur Y, Riess I, 1999. Self-compensation in semiconductors. Physical Review B, 60, pp 8138–8146.

Uihlein C, Frölich D, Kenklies R, 1981. Investigation of exciton fine structure in Cu_2O. Physical Review B, 23, pp 2731–2740.

Vanderbilt D, 1990. Soft self-consistent pseudopotentials in a generalized eigenvalue formalism. Physical Review B, 41, pp 7892–7895.

Vanderbilt D, 1992. Phase segregation and work-function variations on metal surfaces: spontaneous formation of periodic domain structures. Surface Science, 268, pp L300–L304.

van Gastel R, Somfai E, van Albada S B, van Saarloos W, Frenken J W M, 2001. Nothing moves a surface: vacancy mediated surface diffusion. Physical Review Letters, 86, pp 1562–1565.

Vosko S H, Wilk L, Nusair M, 1980. Accurate spin-dependent electron liquid correlation energies for local spin density calculations: a critical analysis. Canadian Journal of Physics, 58, pp 1200–1211.

Wagner C, Hammen H, 1938. Conductivity and oxygen excess in cuprous oxide. Zeitschrift für Physikalische Chemie, 40, pp 197–206.

Wagner C, Schottky W, 1930. Theory of regular mixed phases. Zeitschrift für Physikalische Chemie, 11, pp 163–210.

Walker A V, Yates J T, 2000. Does cuprous oxide photosplit water? Journal of Physical Chemistry B, 104, pp 9038–9043.

Walko D A, Robinson I K, 2001. Energetics of oxygen-induced faceting on Cu(115). Physical Review B, 64, 045412. doi:10.1103/PhysRevB.64.045412

Wang S-H, Schwarz W H E, 2000. On closed-shell interactions, polar covalences, d shell holes, and direct images of orbitals: the case of cuprite. Angewandte Chemie International Edition, 39, pp 1757–1762.

Wang W, Wu D, Zhang Q, Wang L, Tao M, 2010. pH-dependence of conduction type in cuprous oxide synthesized from solution. Journal of Applied Physics, 107, 123717. doi:10.1063/1.3452383

Waugh K C, 2004. The absorption and locking-in of hydrogen in copper. Solid State Ionics, 168, pp 327–342.

Weichman F L, 1960. Photoconductivity of cuprous oxide in relation to its other semiconducting properties. Physical Review, 117, pp 998–1002.

Wells A F, 1984. Structural inorganic chemistry. 5th ed. Oxford: Clarendon.

Werner A, Hochheimer H D, 1982. High-pressure X-ray study of Cu_2O and Ag_2O. Physical Review B, 25, pp 5929–5934.

Wiame F, Maurice V, Marcus P, 2007. Initial stages of oxidation of Cu(111). Surface Science, 601, pp 1193–1204.

Wieder H, Czanderna A W, 1962. The oxidation of copper films to $CuO_{0.67}$. Journal of Physical Chemistry, 66, pp 816–821.

Wright A F, Nelson J S, 2002. Theory of the copper vacancy in cuprous oxide. Journal of Applied Physics, 92, 5849–5851.

Xue J, Dieckmann R, 1990. The non-stoichiometry and the point defect structure of cuprous oxide ($Cu_{2-\delta}O$). Journal of Physics and Chemistry of Solids, 51, pp 1263–1275.

Yagyu K, Nakatsuji K, Yoshimoto Y, Tsuneyuki S, Komori F, 2007. Nanopattern formation on Cu(001) surface coadsorbed with nitrogen and oxygen. Surface Science, 601, pp 4837–4842.

Yagyu K, Liu X, Yoshimoto Y, Nakatsuji K, Komori F, 2009. Dissociative adsorption of oxygen on clean Cu(001) surface. Journal of Physical Chemistry C, 113, pp 5541–5546.

Yamamoto S, Andersson K, Bluhm H, Ketteler G, Starr D E, Schiros T, Ogasawara H, Pettersson L G M, Salmeron M, Nilsson A, 2007. Hydroxyl-induced wetting of metals by water at near-ambient conditions. Journal of Physical Chemistry C, 111, pp 7848–7850.

Yata M, Rouch H, Nakamura K, 1997. Kinetics of oxygen surfactant in Cu(001) homoepitaxial growth. Physical Review B, 56, pp 10579–10584.

Yu P Y, Shen Y R, 1975. Resonance raman studies in Cu_2O. I. The phonon-assisted 1s yellow excitonic absorption edge. Physical Review B, 12, pp 1377–1394.

Yu P Y, Shen Y R, 1978. Resonance raman studies in Cu_2O. II. The yellow and green exciton series. Physical Review B, 17, pp 4017–4030.

Zeppenfeld P, Krzyzowski M, Romainczyk C, Comsa G, Lagally M G, 1994. Size relation for surface systems with long-range interactions. Physical Review Letters, 72, pp 2737–2740.

Zhou G, Yang J C, 2003. Initial oxidation kinetics of copper (110) film investigated by in situ UHV-TEM. Surface Science, 531, pp 359–367.

Zhu Y, Mimura K, Isshiki M, 2004. Purity effect on oxidation kinetics of copper at 800-1050°C. Journal of the Electrochemical Society, 151, pp B27–B32.

Zuo J M, Kim M, O'Keeffe M, Spence J C H, 1999. Direct observation of d-orbital holes and Cu-Cu bonding in Cu_2O. Nature, 401, pp 49–52.

Åsbrink S, Norrby L-J, 1970. A refinement of the crystal structure of copper(II) oxide with a discussion of some exceptional e.s.d.'s (estimated standard deviations). Acta Crystallographica Section B, 26, pp 8–15.

Önsten A, Månsson M, Claesson T, Muro T, Matsushita T, Nakamura T, Kinoshita T, Karlsson U O, Tjernberg O, 2007. Probing the valence band structure of Cu_2O using high-energy angle-resolved photoelectron spectroscopy. Physical Review B, 76, 115127. doi:10.1103/PhysRevB.76.115127

Önsten A, Göthelid M, Karlsson U O, 2009. Atomic structure of $Cu_2O(111)$. Surface Science, 603, pp 257–264.